Tectonics

RESEARCH ARTICLE
10.1029/2020TC006394

**Key Points:**
- Analysis of deformation in northwestern Argentina reveals that numerous, widely distributed, localized structures accommodate shortening
- No well-defined deformation front or clear indication of a locked décollement underlying the region exists
- This behavior is fundamentally different from the thin-skinned fold-and-thrust belt of southern Bolivia and northernmost Argentina

**Supporting Information:**
- Supporting Information S1

**Correspondence to:**
S. Figueroa,
sarafigueroav@gmail.com

**Citation:**
Figueroa, S., Weiss, J. R., Hongn, F., Pingel, H., Escalante, L., Elías, L., et al. (2021). Late Pleistocene to recent deformation in the thick-skinned fold-and-thrust belt of northwestern Argentina (central Calchaquí Valley, 26°S). *Tectonics*, *40*, e2020TC006394. https://doi.org/10.1029/2020TC006394

Received 12 JUN 2020
Accepted 29 NOV 2020
Accepted article online 6 DEC 2020



# Late Pleistocene to Recent Deformation in the Thick-Skinned Fold-and-Thrust Belt of Northwestern Argentina (Central Calchaquí Valley, 26°S)

**Sara Figueroa[1,2], Jonathan R. Weiss[2], Fernando Hongn[1], Heiko Pingel[2], Leonardo Escalante[1], Leonardo Elías[1], R. Germán Aranda-Viana[1], and Manfred R. Strecker[2]**

[1]Instituto de Bio y Geociencias del NOA, Universidad Nacional de Salta-CONICET, Salta, Argentina, [2]Institute of Geosciences, University of Potsdam, Potsdam, Germany

**Abstract** The thick-skinned fold-and-thrust belt on the eastern flank of the Andean Plateau in northwestern Argentina (NWA) is a zone of active contractional deformation characterized by fault-bounded mountain ranges with no systematic spatiotemporal pattern of tectonic activity. In contrast, the thin-skinned Subandean fold-and-thrust belt of northern Argentina and southern Bolivia is characterized primarily by in-sequence (i.e., west to east) fault progression, with a narrow zone of Quaternary deformation focused at the front of the orogenic wedge. To better understand how recent deformation is accommodated across these mountain ranges and the Argentinian portion of the orogen in particular, estimating and comparing deformation rates and patterns across different timescales is essential. We present Late Pleistocene shortening rates for the central Calchaquí intermontane valley in NWA associated with at least three episodes of deformation. Global Positioning System data for the same region reveal a gradual decrease in horizontal surface velocities from the Eastern Cordillera toward the foreland, which contrasts with the rapid velocity gradient associated with a locked décollement in the Subandean Ranges of southern Bolivia. Our new results represent a small view of regional deformation that, when considered in combination with the shallow crustal seismicity and decadal-scale surface velocities, support the notion that strain release in NWA is associated with numerous slowly deforming structures that are distributed throughout the orogen.

## 1. Introduction

Studies of orogenic wedges and adjacent foreland basins often focus on thin-skinned fold-and-thrust belts, where accommodation space is created by the flexural response of the crust to the topographic load of the advancing mountain belt and orogenic wedge (e.g., DeCelles & Giles, 1996; Jordan, 1981). In these systems, deformation generally progresses toward the foreland with a well-defined deformation front, incorporating progressively younger sediments. Strain in these structural settings is thought to accumulate along deep portions of a gently dipping basal décollement; close to the surface, however, the décollement commonly remains locked until the accumulated strain is released in earthquakes that propagate toward the tip of the orogenic wedge (e.g., Avouac, 2008; Brooks et al., 2011; Hubbard et al., 2015; Weiss et al., 2015). In contrast, in thick-skinned fold-and-thrust belts and broken forelands with spatially isolated fault-bounded ranges, active shortening is often associated with the reactivation of high-angle basement structures (DeCelles & Giles, 1996; Jordan & Allmendinger, 1986; Marshak et al., 2000), which results in widely distributed and often disconnected fault-bounded basins and associated ranges with a poorly defined or absent deformation front (e.g., Hilley et al., 2005; Strecker et al., 2012). These two contrasting, end-member tectonic settings exist in the adjacent thin-skinned Subandean fold-and-thrust belt of southern Bolivia and the thick-skinned fold-and-thrust belt of northwestern Argentina (NWA) (Figure 1). The close proximity of these morphotectonic provinces to each other provides an excellent opportunity to compare tectonic deformation rates and styles within the same regional geodynamic framework over different timescales.

The thick-skinned fold-and-thrust belt of NWA comprises the basement-cored uplifts of the Eastern Cordillera (EC) and the Santa Bárbara System (SBS) (Figure 1) that form unconnected topographic

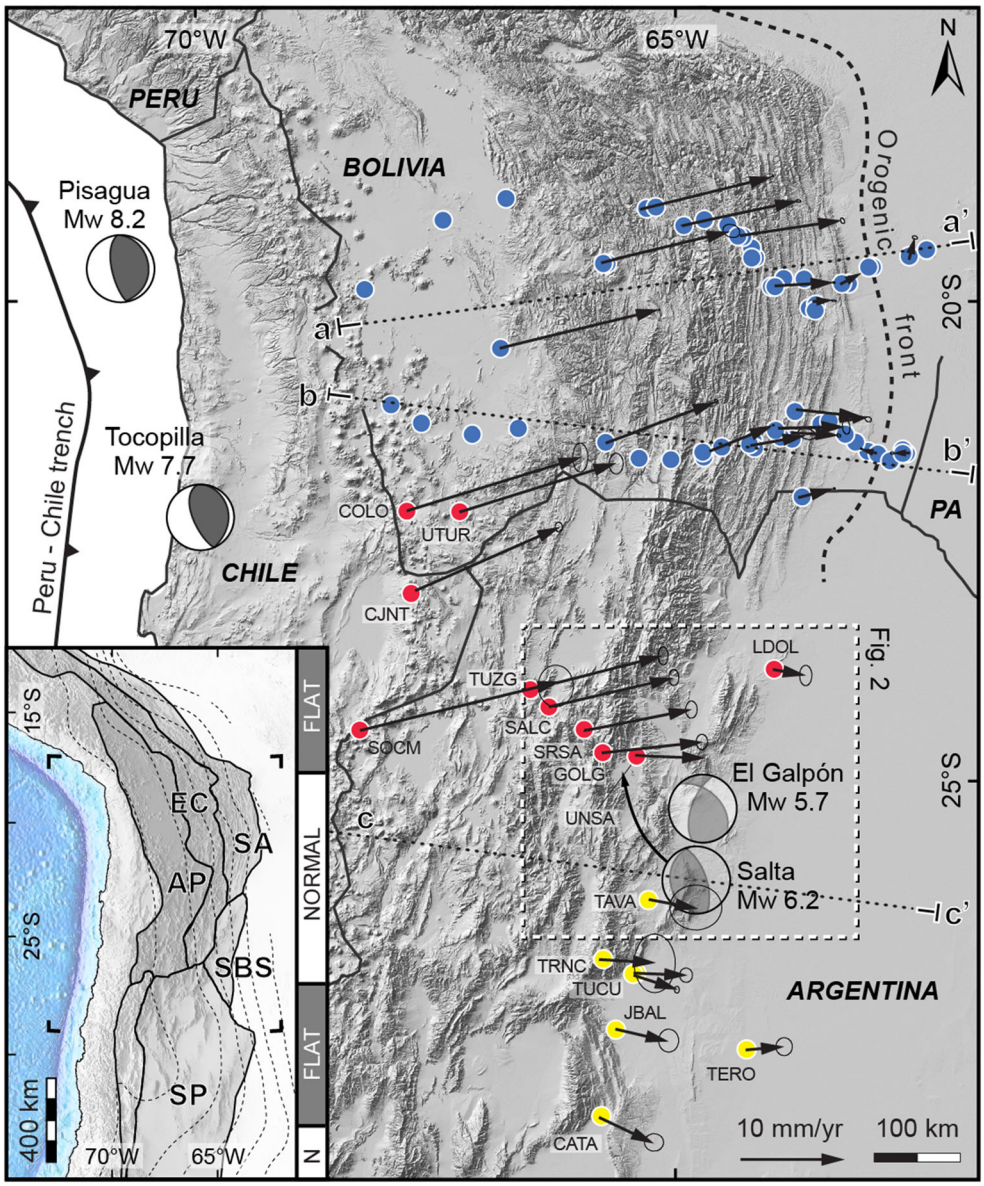


**Figure 1.** Topography and GPS-derived surface velocities for the Central Andean region. Blue circles indicate GPS sites in Bolivia from Weiss et al. (2016) with CGPS horizontal velocity vectors and 2-sigma error ellipses. Red circles are NWA CGPS site locations from McFarland et al. (2017) with revised horizontal velocities from this study. Yellow CGPS velocities are newly added. Also shown are focal mechanisms for recent earthquakes that affect the GPS time series. Note the contrasting topography associated with the thin- and thick-skinned fold-and-thrust belts of southern Bolivia and NWA. Inset shows the Central Andean principal morphotectonic provinces discussed in the text after Eude et al. (2015), Strecker et al. (2007), and Jordan et al. (1983) and dashed 100-km-interval Nazca plate contours from Slab2 (Hayes et al., 2018) with flat-slab and normal-dip segments indicated to the right. EC = Eastern Cordillera; SA = Subandes, AP = Altiplano-Puna Plateau; SBS = Santa Bárbara System; SP = Sierras Pampeanas.

barriers and intervening intermontane basins (González Bonorino, 1950a; Kley et al., 2005; Mon & Salfity, 1995). The barriers control unsystematic fluvial and sediment-routing systems characteristic of broken forelands (Grier et al., 1991; Hain et al., 2011) and are located to the east of the high, internally drained Andean Plateau, which is also known as the Puna Plateau in Argentina. The generally north-south oriented ranges of the EC and SBS are often associated with reactivated basement structures inherited from Cretaceous extensional processes in the Salta Rift (Carrera et al., 2006; Iaffa et al., 2011; Kley et al., 2005; Kley & Monaldi, 2002). The ranges are bounded by either westward or eastward verging thrust and reverse faults (Mon & Salfity, 1995) (Figures 1 and 2). The imprint of the pre-Andean

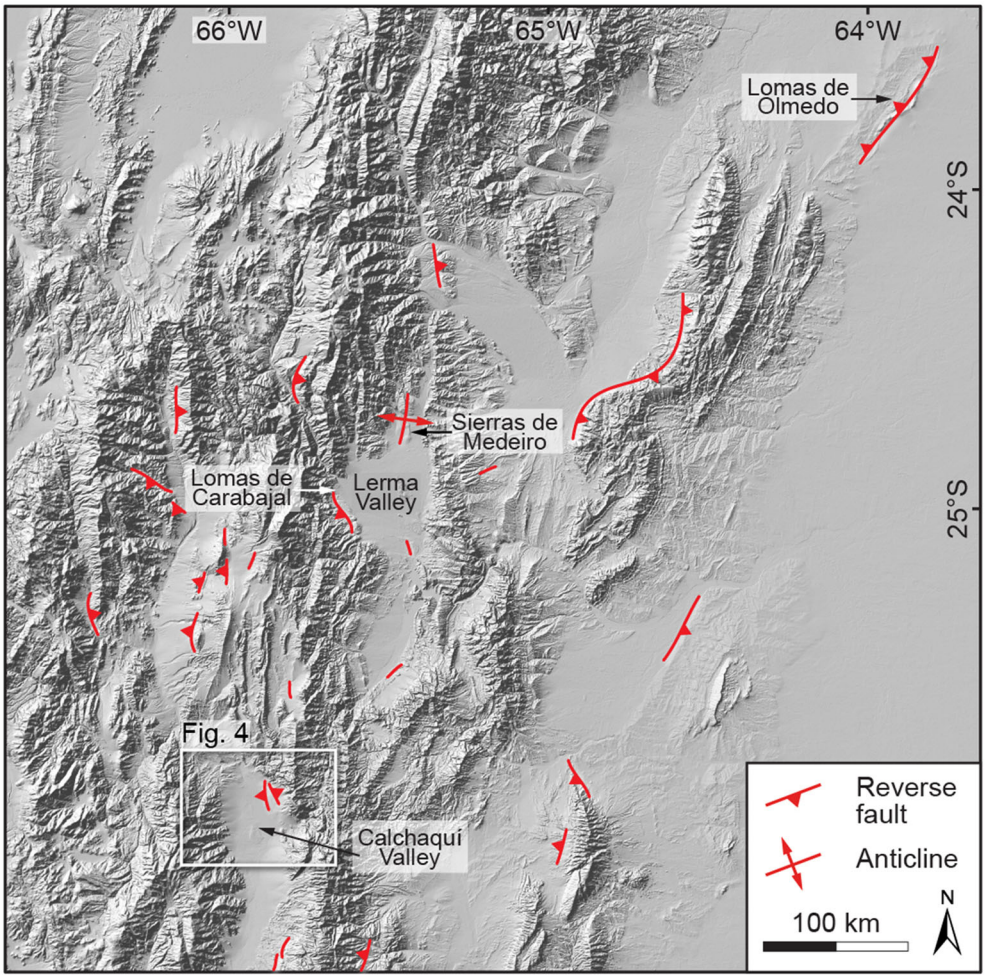


**Figure 2.** Shaded relief map of the study area with Quaternary faults and structures after Casa et al. (2014). Locations described in the text are labeled.

paleogeography on the accommodation of Cenozoic shortening is reflected by a broad zone of deformation with widely distributed Quaternary faults and folds. In addition, the mountain ranges in this region record unsystematic lateral growth through time and a well-defined, active orogenic front does not exist (García et al., 2019; Hain et al., 2011; Mortimer et al., 2007; Ramos et al., 2006; Reynolds et al., 2000; Strecker et al., 2012). This sharply contrasts with the style of deformation in the adjacent Subandean fold-and-thrust belt to the north, which is generally characterized by the eastward younging of geological structures and intermontane sedimentary basins that have formed in the hanging walls of individual thrust sheets (e.g., Dunn et al., 1995; Echavarria et al., 2003; Mugnier et al., 2006; Uba et al., 2009).

The contrast in structural styles between the two fold-and-thrust belts was originally ascribed to along-strike variations in the subduction angle of the Nazca plate beneath the western margin of South America (Jordan et al., 1983) (Figure 1). Subduction is steep (~30°) in southern Bolivia, but a gradual decrease in slab dip occurs moving southward, and a well-defined, nearly horizontal, flat-slab segment exists beneath the reverse-fault bounded Sierras Pampeanas of central Argentina between about 27°S and 33°S (Jordan et al., 1983). However, the structural styles in the foreland areas are transitional between differently dipping sectors of the subducting Nazca plate, and a correlation between upper-plate deformation and subduction angle is poor (Kley et al., 1999).

The difference in structural style between the thick- and thin-skinned fold-and-thrust belts is evident in instrumentally recorded seismicity. Shallow (<40 km) earthquakes in NWA ranging in magnitude from

$M_w$ 2–7 are numerous and widely distributed, whereas in Bolivia there have been only a few crustal earthquakes, primarily located at the deformation front (see section 5) (Storchak et al., 2013).

Despite the fully studied structural characteristics of the thick-skinned fold-and-thrust belt and broken foreland in NWA, details of the overall seismotectonic behavior are scarce and remain poorly understood. Using regional structural mapping and geochronology, Pearson et al. (2013) calculated shortening rates of 1.9 mm/yr from 40 to 12 Ma, 6.5 mm/yr from 12 to 4 Ma, and 5.3 mm/yr from 4 Ma to recent, resulting in a time-averaged, long-term shortening rate of 3.6 mm/yr for the last 40 Myr between the latitudes of 25–26°S. García et al. (2013) determined Holocene shortening rates of ~2 mm/yr in the Lerma Valley, and Ramos et al. (2006) calculated a Holocene shortening rate of 2.34 mm/yr farther east in the Lomas de Olmedo (Figure 2). This contrasts with the thin-skinned fold-and-thrust belt to the north, where McQuarrie et al. (2008) determined long-term shortening rates of 4–8 mm/yr, and Echavarria et al. (2003) calculated Quaternary shortening rates of 8–11 mm/yr. In light of these studies and observations suggesting that deformation in the SBS and EC is widely distributed in space and time (García et al., 2019; Hain et al., 2011; Reynolds et al., 2000), it appears that the Quaternary tectonic shortening rates in the thick-skinned fold-and-thrust belt differ from the long-term rates, whereas comparable long- and short-term deformation rates characterize the thin-skinned sector of the orogen.

Active deformation across the Central Andes has been measured at the decadal scale using the Global Positioning System (GPS) (Brooks et al., 2011; McFarland et al., 2017; Norabuena et al., 1998; Villegas-Lanza et al., 2016; Weiss et al., 2016). Three recent studies have focused specifically on the Central Andean backarc: Brooks et al. (2011) and Weiss et al. (2016) analyzed data from Bolivia spanning the Andean Plateau (Altiplano), EC, and Subandean fold-and-thrust belt, whereas McFarland et al. (2017) focused on a transect from the Chilean Precordillera to the SBS. Despite the structural differences between the two locations, at first glance the overall shapes of GPS-derived, horizontal surface-velocity profiles reveal a similar rapid decrease from ~6–12 mm/yr in the west to ~0 mm/yr in the east over distances ranging from ~35–100 km, suggesting comparable crustal shortening kinematics (Figures 1 and 3).

In light of the observed differences in styles and rates of deformation, the goals of this study are to better illuminate how deformation is accommodated across these regions and to determine whether the deformation has been consistent through time. To achieve these goals, we calculate Middle-Late Pleistocene shortening rates for the central intermontane Calchaquí Valley in the thick-skinned sector of the Andean orogen in NWA (Figures 1, 2, and 4), relate these observations to revised geodetically determined surface-velocity estimates and upper crustal seismicity, and compare our results with those from the adjacent thin-skinned Subandean fold-and-thrust belt to the north and thick-skinned Sierras Pampeanas to the south.

## 2. Geological Setting

The fault-bounded intermontane central Calchaquí Valley is located at the confluence of the Calchaquí and Santa María rivers in the vicinity of the town of Cafayate, in the southeastern sector of the EC of NWA (Figure 4). The region lies to the east of the Puna plateau, at the intersection of the EC, Sierras Pampeanas, and SBS (Grier et al., 1991; Ramos, 2017) (Figure 1). A common feature of these morphotectonic provinces is the influence of inherited structures on the evolution of foreland deformation, which has resulted in primarily thick-skinned deformation, widely distributed Quaternary deformation, and recent seismicity (Alvarado & Ramos, 2011; Carrera & Muñoz, 2013; Costa et al., 2018; González Bonorino, 1950b; Hongn et al., 2010; Strecker et al., 2012).

Recent deformation in the central Calchaquí Valley is mainly controlled by the reactivation of inherited lower Paleozoic and Cretaceous basement structures (Grier et al., 1991; Hongn et al., 2010). For example, the orientation of exhumed Cretaceous normal faults is closely aligned with Paleozoic basement heterogeneities (Hongn et al., 2010) and Cenozoic mountain building reactivated or inverted the Cretaceous extensional structures, leading to basement-cored mountain ranges with partially connected depocenters (Carrera et al., 2006; del Papa et al., 2013; Mon & Salfity, 1995). This reactivation contributes to the predominantly west vergent orientation of structures in the Calchaquí Valley (Carrera & Muñoz, 2008; Grier et al., 1991; Hongn et al., 2010; Mon & Salfity, 1995).

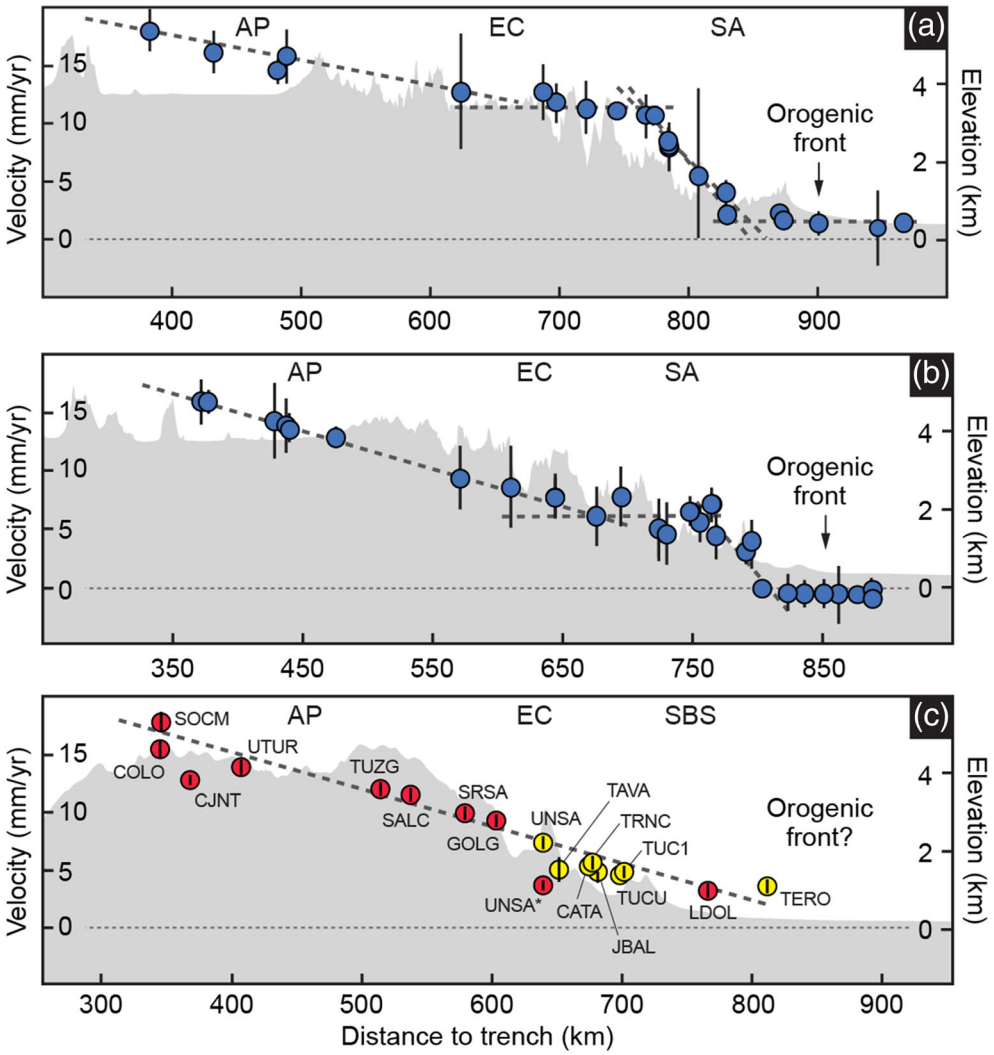


**Figure 3.** Structure-perpendicular elevation and velocity profiles for (a and b) the Subandes from Weiss et al. (2016) and for (c) NWA. Filled circles and 2-sigma error bars are projected horizontal velocities. Note that in many cases the error bars for CGPS sites are smaller than the circles. In profile (c) error bars are plotted in front of the circles. Gray dashed lines are hand-drawn fits to the data intended to emphasize features in the velocity field that we refer to in the text. Two velocities for UNSA are shown in (c) with the smaller value (UNSA*) corresponding to the interseismic velocity estimate from McFarland et al. (2017) and the revised, larger value from this study. Note the rapid decrease in velocity between GOLG and UNSA does not exist if our revised estimate is considered. See main text for additional details.

Here we focus on the eastern fluvial outlet of the central Calchaquí Valley (Figures 1 and 3), where the inverted El Zorrito and Los Castillos en echelon border faults have uplifted and deformed Cretaceous synrift units (Pirgua Subgroup-Salta Group) that constitute the León Muerto range (Carrera & Muñoz, 2013; Marquillas et al., 2005). To the west, the studied sector of the basin is bordered by Neoproterozoic-Lower Paleozoic igneous-metamorphic basement rocks of the Quilmes Range (Büttner et al., 2005). East of the basin, Late Cretaceous-Paleogene post-rift sediments of the Salta Group and foreland-basin deposits of the Paleogene to Neogene Payogastilla Group are exposed (Carrera et al., 2006; Carrera & Muñoz, 2013). These deformed and incised units are unconformably covered by Quaternary fluvial, alluvial, and lacustrine deposits (Gallardo, 1988; Hermanns & Strecker, 1999) that are well exposed in the piedmont of the León Muerto range (Figure 4) and on the flanks of the basement-cored El Mollar anticline (Figure 4). Gallardo (1988) defined four Quaternary lithostratigraphic units in this region, but here we adopt

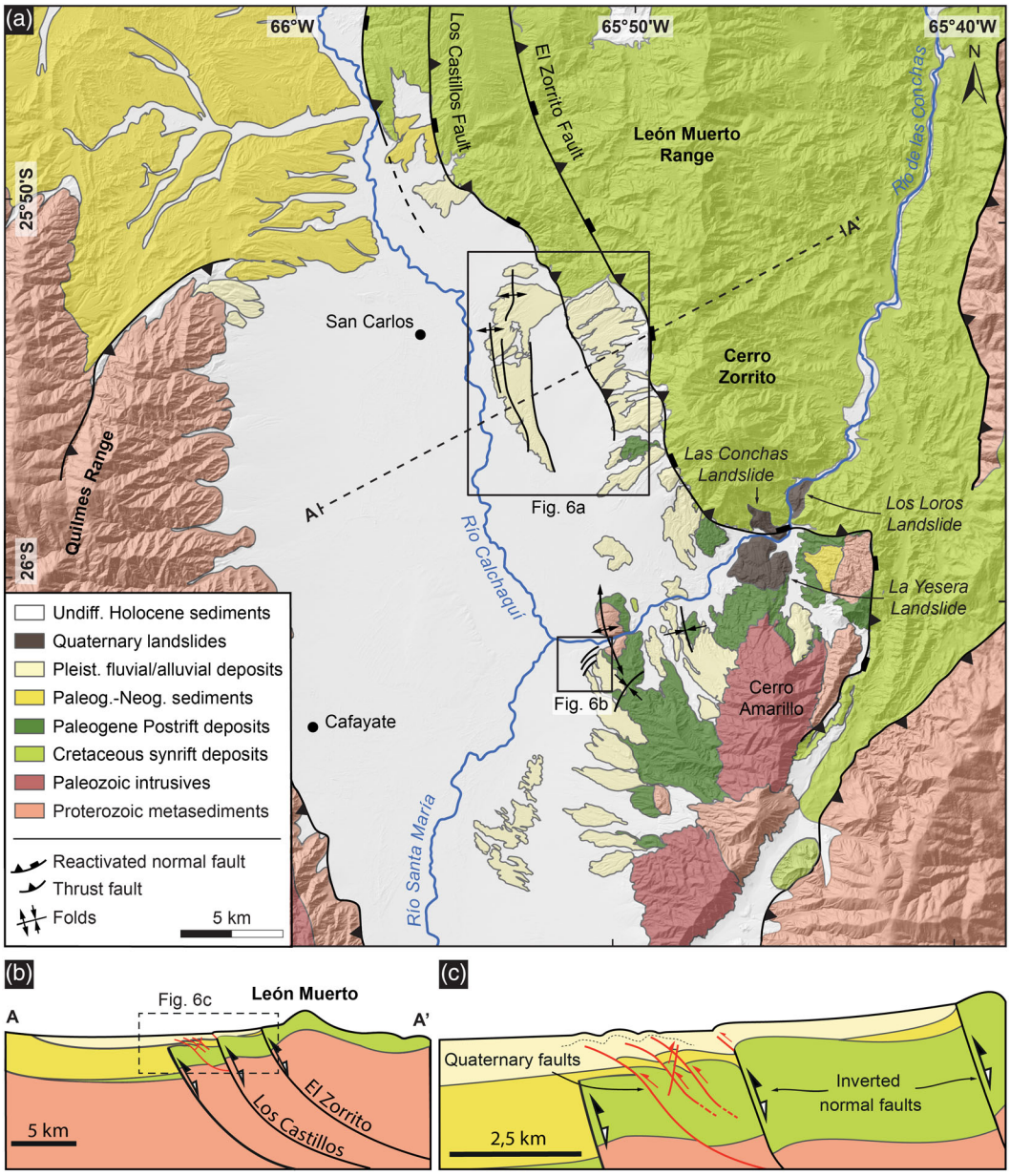


**Figure 4.** Geologic map and structural cross sections of the study area in the Central Calchaquí Valley; see Figure 3 for location. (a) Geological map with major, valley-border faults and the location of Las Conchas and Los Loros landslides that impounded the Las Conchas river valley and caused the lacustrine deposits of the El Paso Formation (Gallardo, 1988; Hermanns & Niedermann, 2011). Black boxes indicate the location of the piedmont of the León Muerto range and the El Mollar area shown in Figure 6. (b and c) Schematic model of the footwall-shortcut faults from the Los Castillos fault from Profile A-A′ showing the relationship between the Quaternary structures and the inverted valley-border faults.

informal units that are tied to sedimentary strata that we dated (see below). Many of these units are folded and faulted. Additional work is required to better document Quaternary stratigraphic relationships and to propose a formal stratigraphy.

Central to our study are deformed lacustrine deposits (intercalated with or overlain by conglomeratic gravel units) that result from the impoundment of the Río de Las Conchas drainage system by voluminous rock-avalanche deposits (Hermanns & Strecker, 1999; Torres, 1985) (Figure 4). Both the landslide and paleolake deposits are dated to 13,550 ± 870 and 15,250 ± 1960 yr BP, respectively, although they may have been

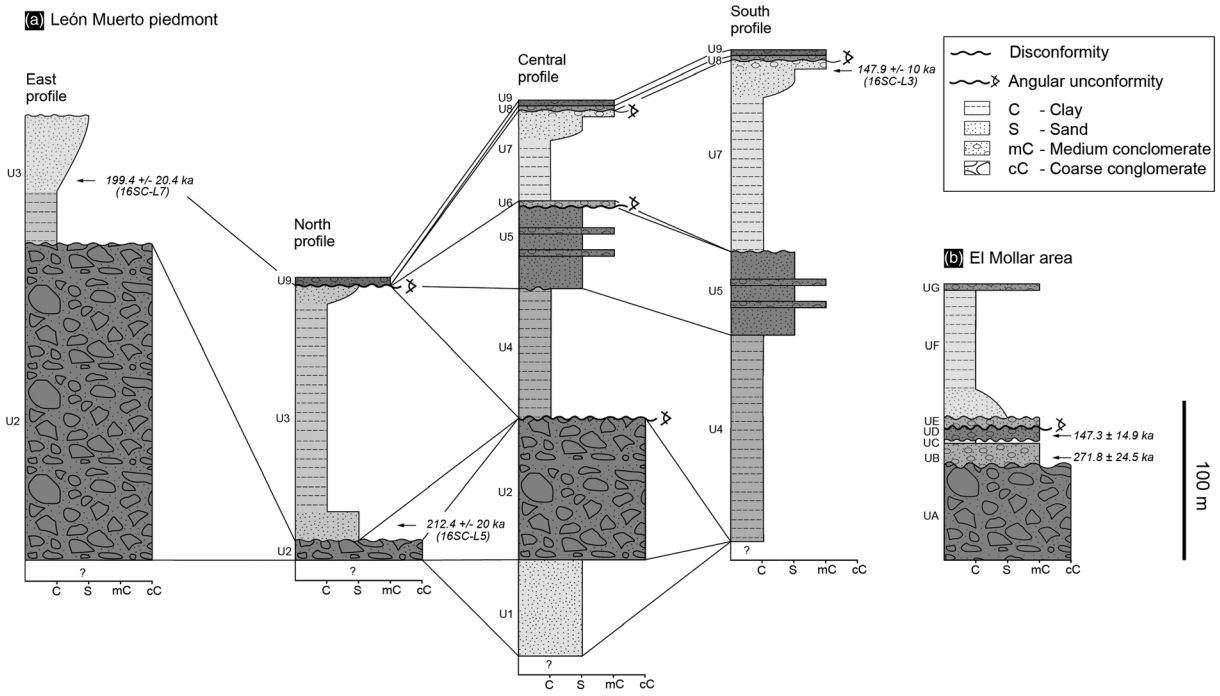


**Figure 5.** Stratigraphy of (a) the piedmont of the León Muerto range from the eastern, northern, central, and southern profiles and (b) the El Mollar area. The ages from the León Muerto range piedmont are from this study, whereas those from the El Mollar area are from Reger (2018). See the SI for additional OSL dating details.

deposited simultaneously at about 13,830 ± 790 yr BP (Hermanns et al., 2004). During a >9,000-year-long period of the lake's existence, lacustrine strata were deposited, some with horizons of convoluted bedding and soft-sediment deformation interpreted as seismites (Hermanns et al., 2004; Hermanns & Niedermann, 2011).

## 3. Methodology

We first analyzed Landsat Enhanced Thematic Mapper imagery and a 12-m-resolution TanDEM-X digital elevation model to guide fieldwork and site selection for structural and stratigraphic mapping of exposed Quaternary deposits. We identified target areas that displayed unambiguous evidence of neotectonic activity in the form of deformed lacustrine marker beds and associated alluvial-fan deposits; we mapped these outcrops and developed a consistent stratigraphy for the piedmont of the León Muerto range and the El Mollar area. We collected three sand samples in the area of the León Muerto range piedmont (16SC-L3, 16SC-L5, and 16SC-L7) for optically stimulated luminescence (OSL) dating (see the supporting information, SI). In addition to our new OSL results (Figure 5 and Table 1), we also rely on OSL data from Reger (2018) (see SI for additional details).

We next determined shortening rates using our new stratigraphic scheme, structural data collected in the field, and geological profile balancing based on the Busk fold-construction method (Busk, 1929), which per-

**Table 1**
*Shortening Rates for Study Areas in the Central Calchaquí Valley, NWA (mm/yr)*

| León Muerto range piedmont | | | El Mollar area | | |
|---|---|---|---|---|---|
| Profile | Busk method | 2-D kinematic model | Profile | Busk method | 2-D kinematic model |
| Northern N-N′ | 1.03–2.80 | 1.05–2.90 | Eastern A-A′ | 0.19–0.24 | 0.52–0.64 |
| Central C-C′ | 0.95–2.63 | 1.64–4.47 | Western B-B′ | 0.21–0.26 | 0.31–0.38 |
| Southern S-S′ | 0.42–1.17 | 1.55–4.20 | | | |
| Eastern E-E′ | | 0.64–1.47 | | | |

mits the creation of cylindrical folds that best fit our field observations, as well as line-length balancing methods for the restoration (e.g., Dahlstrom, 1969). The profiles based on the Busk method only consider the field observations at the surface and therefore represent minimum deformation estimates. To address the possibility of blind structures underlying some of the folds, we also conducted 2-D kinematic modeling using the MOVE software package to generate area-balanced structural models. Due to a lack of subsurface data and the presence of numerous unconformities, we treat the Quaternary sediments as a single package; we mapped and inferred field geometries and fault parameters, including morphology, assumed kinematics, slip, and the angle of trishear in order to derive basic models that best fit our structural data (Figure S2). In contrast to the Busk models, we consider these 2-D kinematic models to represent a maximum amount of shortening. Shortening rates were calculated using shortening-magnitude estimates obtained from the Busk reconstructions, by unfolding the strata because fault slip was unknown, and using the kinematic model-derived fault-slip estimates, in combination with the time interval corresponding to the deposition of the units (Table 1).

To supplement our Quaternary shortening-rate estimates, we derived surface-displacement time series and interseismic surface velocities using a regional network of continuously recording GPS (CGPS) sites following the methods described in Weiss et al. (2016) (Figure 1) while paying close attention to perturbations from long-term "interseismic" displacement trajectories and rates due to subduction zone as well as local earthquake coseismic and postseismic affects. We constructed velocity profiles along a WNW-ESE transect, perpendicular to the strike of the majority of the recently active structures at this latitude (Figure 1). The GPS-derived surface velocities contribute to our understanding of the kinematics of decadal-scale deformation across the thick-skinned sector of the orogen and facilitate a comparison with the longer-term shortening rates during the Quaternary that are based on fieldwork and published tectonic shortening rates.

## 4. Results

### 4.1. Stratigraphy

In the piedmont of the León Muerto range, we identified nine Quaternary units (Units 1 to 9; Figure 5). For simplicity, we only show the most prominent, widely distributed units that can be distinguished on satellite images (Figure 6a) and we present stratigraphic sections for four associated profiles (Figure 5). The units consist of intercalated alluvial-fan conglomerates, fluvial sands, and lacustrine clayey silts that are exposed with mappable lateral extent. We attribute significant lateral changes in unit thickness to a combination of a highly dynamic, variable depositional environment in transitional sectors of the piedmont between fluvial, alluvial-fan, and lacustrine settings. Complex facies relationships, lateral pinch-outs, and superposition of strata in this environment also result from both the flow direction of the Calchaquí river and the effects of focused deformation, uplift, and concomitant fluvial erosion. In the El Mollar area we mapped seven units (Units A to G, Figure 5). Detailed descriptions of the mapped units and regionally important units that are only exposed in vertical erosional cuts, as well as information on sampling locations, can also be found in the SI.

### 4.2. Chronostratigraphy

The ages of three samples from the León Muerto range piedmont area were determined using OSL dating (Figure 5 and Table 1), which yielded ages of 147.9 $\pm$ 10 ka (16SC-L3, Unit 7), 212.4 $\pm$ 20.1 ka (16SC-L5, Unit 3), and 199.4 $\pm$ 20.4 ka (16SC-L7, Unit 3). Both 16SC-L5 and 16SC-L7 correspond to Unit 3.

### 4.3. Quaternary Deformation

Quaternary deformation in the central Calchaquí Valley is associated with the formation of new structures within the valley and the reactivation of the basin-bounding El Zorrito-Los Castillos fault system (Figures 4 and 6a). Numerous north striking, primarily east dipping faults are located in the piedmont of the León Muerto range. In contrast, most of the structures in the El Mollar area strike NE-SW and dip to the southeast (Figures 4 and 6b).

#### 4.3.1. Piedmont Sectors of the León Muerto Range

We analyzed four structural profiles in the piedmont of the León Muerto range (Figure 6a). The Busk reconstructions result in three asymmetric anticlines in the northern profile that disappear to the south (Figure 7). The central and southern profiles are characterized by five and three folds, respectively. In both profiles, the

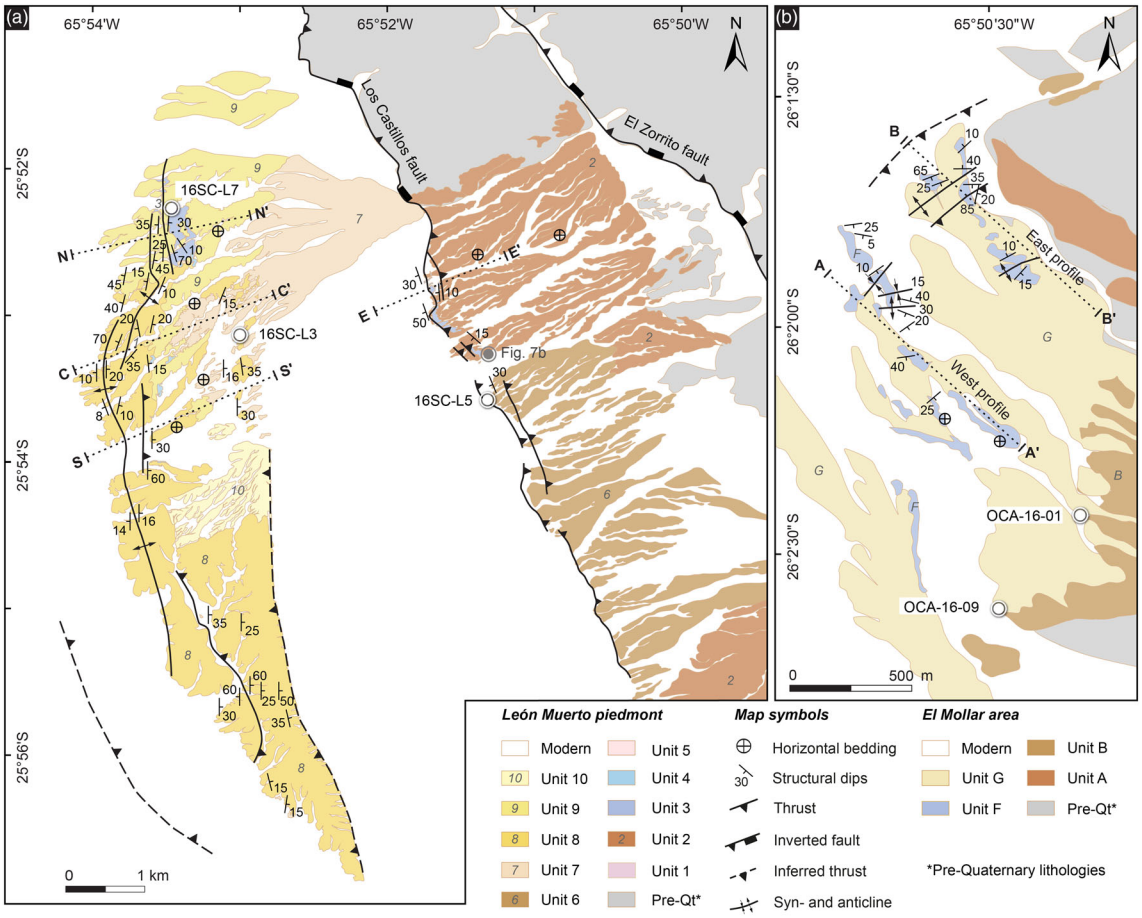


**Figure 6.** Quaternary geological and structural map for (a) the piedmont of the León Muerto Range and (b) the El Mollar area. White circles indicate OSL sample locations. Black dotted lines indicate the locations of the structural profiles shown in Figures 7, 8, and S3.

western anticline is formed by Unit 5 (Figure 7d). Toward the east of the central profile, a syncline-anticline pair is observed in Units 1 and 2. These structures also disappear southward, but the central anticline formed by Unit 4 is a fold associated with the outcropping fault in the southern profile (Figure 7f). The easternmost fold in the central and southern profiles is an east dipping monocline formed by Unit 7, which lies unconformably above Unit 4 (Figure 7e). The eastern profile has not been reconstructed using the Busk method because it crosses the Los Castillos fault scarp and the observed changes in dip associated with the offset and deformed strata are more suitable for 2-D kinematic modeling.

The model reconstructions (Figure S2) suggest that the anticlines are probably generated by fault-propagation folding suitable for modeling using the trishear approach. The structures in the southern and central profiles were modeled as west verging with the exception of the easternmost fault and associated monocline, which we modeled as a high-angle, east verging fault. To the north, the anticlines were modeled as east verging, blind fault-propagation folds with trishear tips that may be back thrusts associated with a deeper, west verging, low-angle fault. The eastern profile was modeled considering the surface fault links directly with the Los Castillos fault at depth (Figures 2 and 6a); it is responsible for the deformation of Units 2 and 3 in a west dipping monocline. Due to the observed pronounced surface deformation and numerous unconformities between the units (Figures 5, 7, and S2), a greater amount of shortening is required in the central profile compared to adjacent regions.

We consider deformation to have occurred between 147.9 ± 10 and 212.4 ± 20.1 ka based on our age determination for Units 3 and 7, resulting in a timespan ranging from 34.4 to 94.6 kyr, which we use for calculating minimum and maximum shortening rates for the north, central, and southern profiles (Table 1). For the eastern profile, considering the lack of age constraints above Unit 3, we use a timespan of 212.2 ± 20.1 kyr,

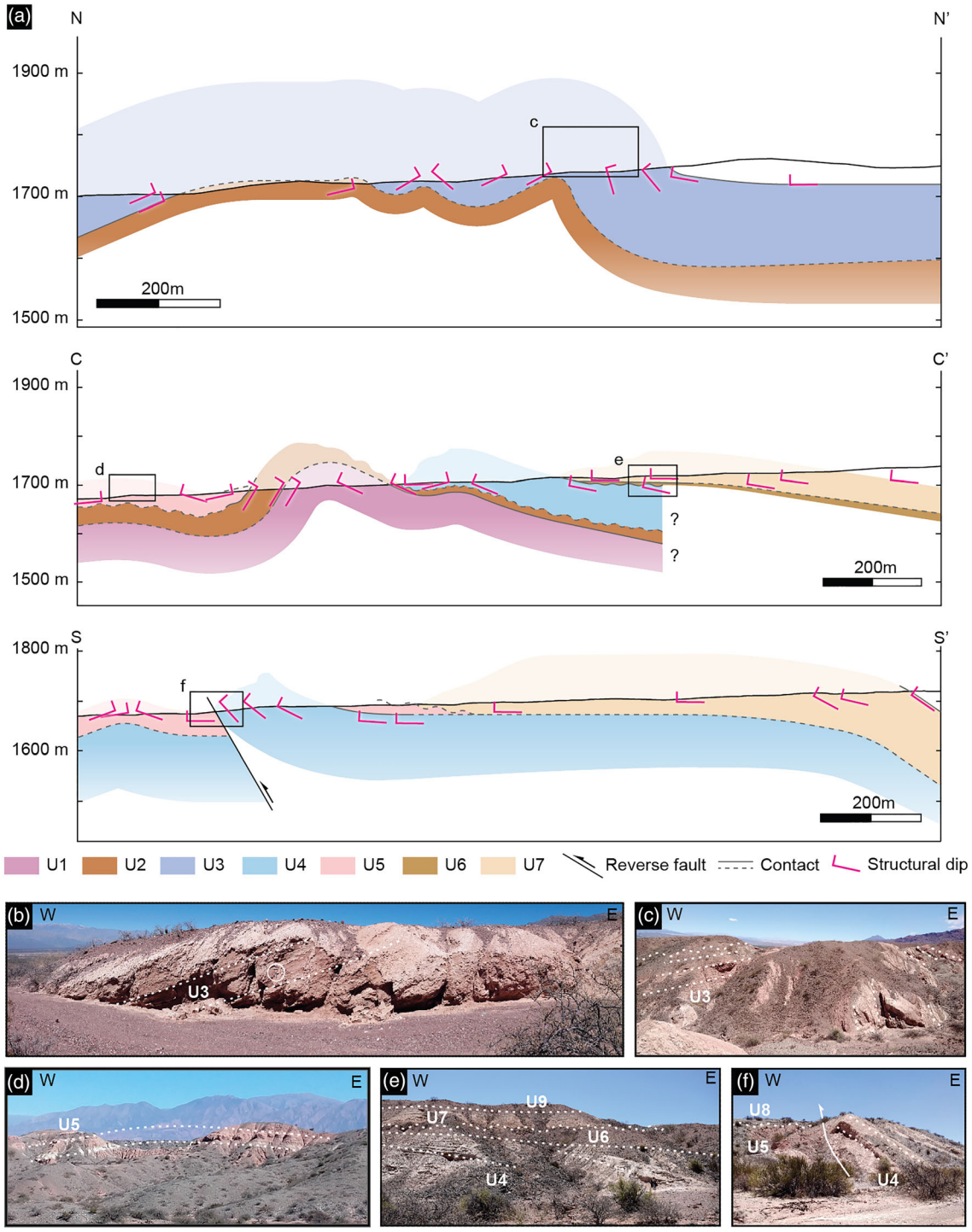


**Figure 7.** Structural profiles and field photos of the piedmont of the León Muerto range. (a) Structural profiles of the piedmont of the Sierra León Muerto based on the Busk method. The missing Units 8 and 9 are not represented in the profile because of the scale. (b–f) View of some of the regional structures exposed along streams. (b) West dipping strata of Unit 3 on the Quaternary scarp of the Los Castillos fault. White circle denotes a rock hammer for scale. Photo location is shown in Figure 6a. (c) Eastern anticline from the northern profile affecting Unit 3. (d) Western anticline on the central profile deforming Unit 5. (e) Angular unconformity between lacustrine Units 7 and 4. (f) Unit 4 thrusted over Unit 5 from the southern profile. Unit 8 covers Unit 5.

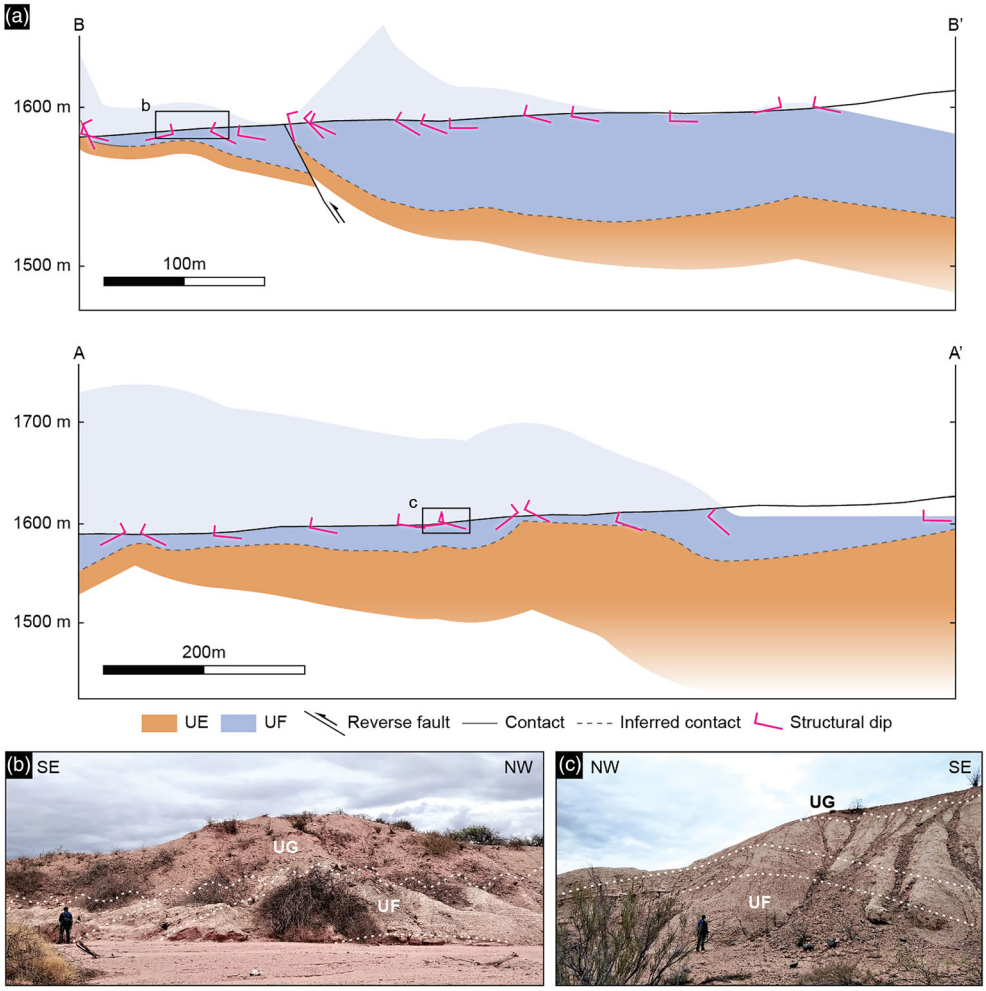


**Figure 8.** (a) Structural profiles from the El Mollar area using the Busk method. (b and c) Field exposures of (b) an anticline from Profile B deforming Unit F and (c) an anticline from profile folding Unit F.

which represents the age of Unit 3 to the present. From the Busk-method reconstructions, we obtained rates of 1.03–2.80 mm/yr for the northern profile, 0.95–2.63 mm/yr for the central profile, and 0.42–1.17 mm/yr for the southern profile. The 2-D kinematic model reconstructions yielded rates of 1.05–2.90, 1.64–4.47, 1.55–4.20, and 0.64–1.47 mm/yr for the northern, central, southern, and eastern profiles, respectively. The large differences between the minimum and maximum shortening rates are related to the age uncertainty.

#### 4.3.2. El Mollar Area

In the El Mollar area, we constructed two parallel, NW-SE oriented profiles (Figure 6b). The Busk reconstructions reveal the general south-dipping trend of the strata and associated with small, local anticlines. (Figures 6b and 8). The kinematic models for both profiles involve two fault-bend folds (Figure S2) with small changes in fault dip responsible for the anticlines observed at the surface. The kinematic models place a detachment horizon at a depth of 400 m below the surface, which may correspond to strata associated with the Paleogene post-rift stratigraphy that are exposed in the vicinity (Carrera et al., 2006).

The deformation affecting Unit F occurred after the deposition of Units A–D, and since no time constraints exist to further refine the deformational timing, we used the age of Unit D (147.3 ± 14.9 kyr) to calculate shortening rates taking into account the uncertainty of the OSL age. Consequently, the associated shortening rates are minimum estimates. The values obtained from the Busk method for the eastern profile are 0.19–0.24 and 0.21–0.26 mm/yr for the western profile. The kinematic model reconstructions result in shortening rates of 0.52–0.64 mm/yr for the eastern profile and 0.31–0.38 mm/yr for the western profile.

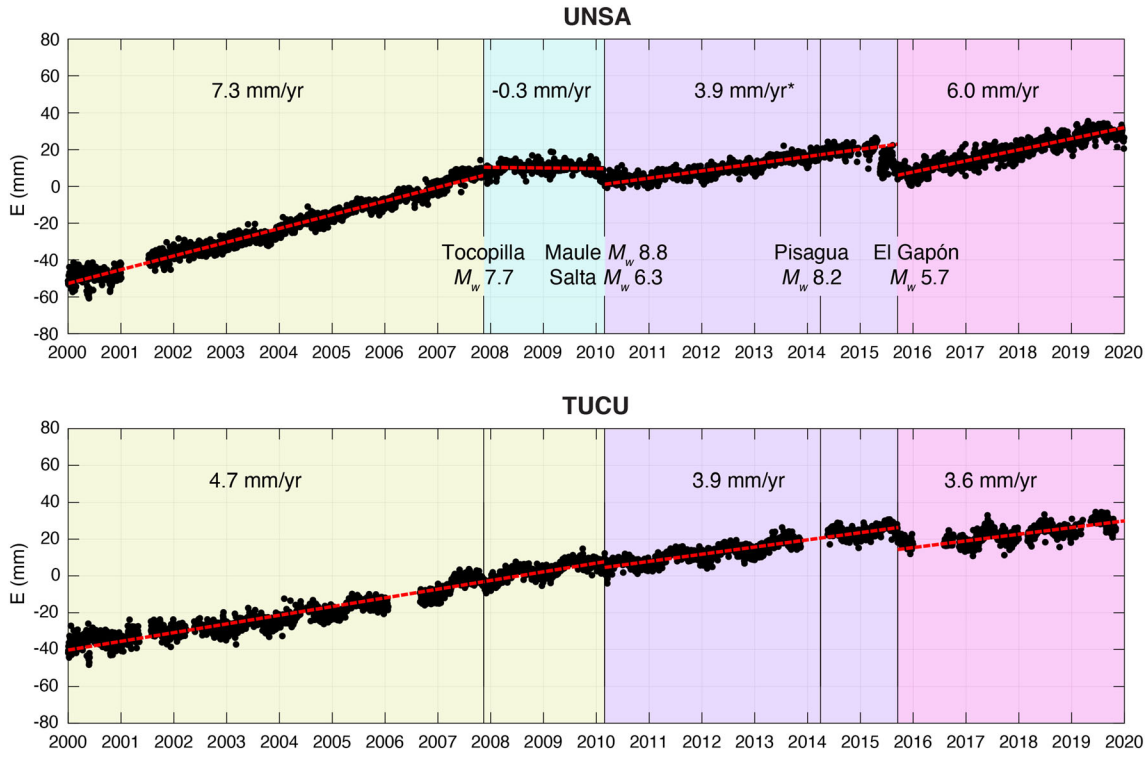


**Figure 9.** East component of the 2000–2020 daily time series for continuous GPS sites UNSA (Universidad de Salta) and TUCU (Tucumán). See Figure 1 for site locations. Red dashed lines are best fitting linear velocities for portions of the time series with no detectable changes in trajectory (i.e., constant velocity intervals). Major earthquakes that affect one or both of the time series are shown as vertical black lines. The colored rectangles represent constant velocity intervals. Note the strong influence that earthquakes exert on the east component of the UNSA time series and corresponding velocities compared to TUCU, where more subtle changes emerge.

### 4.4. Geodetic Observations of Active Shortening

GPS-derived horizontal surface velocities projected onto a structure-perpendicular profile in NWA gradually decrease from west to east (Figure 1). A similar velocity profile presented in McFarland et al. (2017) located slightly to the north of our new profile exhibits an abrupt velocity decrease between the CGPS site near the Golgóta fault (GOLG) (Strecker & Marrett, 1999) and the Universidad de Salta site (UNSA) (Figure 1) superposed on the overall pattern of a gradual eastward velocity reduction. As we discuss below, the abrupt change is used by McFarland et al. (2017) to argue for the presence of a locked décollement underlying the ranges of the EC, similar to what has been observed in the fold-and-thrust belt of southern Bolivia (Brooks et al., 2011; Weiss et al., 2016). The rapid decrease in structure-perpendicular velocities from ~10 mm/yr at GOLG to ~4 mm/yr at UNSA presented in (McFarland et al., 2017) occurs over a distance of ~20 km and is largely defined by the velocity at UNSA (Figure 1), where the eastward component of the displacement time series is heavily affected by megathrust and backarc earthquakes including the Tocopilla, Maule, Pisagua, and El Galpón events (Figure 9). McFarland et al. (2017) used UNSA surface-displacement data from a 4-year time interval between the 2010 $M_w$ 8.8 Maule and the 2014 $M_w$ 8.1 Pisagua earthquakes to define the interseismic velocity shown in their profile. We caution that the displacements from this time interval may not be representative of the interseismic rate and result in a mischaracterization of the regional kinematics.

Our analysis of the CGPS daily displacement time series for UNSA reveals multiple changes in trajectory (i.e., velocity) that appear to be associated with major earthquakes (Figures 9 and S1). For example, for the time interval between early 2000 and the 2007 $M_w$ 7.7 Tocopilla earthquake (Delouis et al., 2009), the station moved steadily eastward at a rate of ~7.3 mm/yr. The eastward velocity decreased abruptly to ~0.3 mm/yr following the Tocopilla event until the 2010 $M_w$ 8.8 Maule and $M_w$ 6.3 Salta earthquakes

(Scott et al., 2014). After the 2010 events, the velocity increased to ~3.9 mm/yr (Figure 9) until just prior to the 2015 $M_w$ 8.3 Illapel, Chile (Grandin et al., 2016), and $M_w$ 5.7 El Galpón, Argentina, earthquakes. Time series perturbations associated with these events make estimating a constant velocity for UNSA difficult during 2015, but the station appears to have resumed steady eastward motion at a rate of ~6.4 mm/yr starting in early 2016, which is close to the pre-Tocopilla interseismic velocity. For comparison, the eastward component of the daily time series for the CGPS site in Tucumán, Argentina (TUCU), at a similar longitude in the thick-skinned broken foreland of the northern Sierras Pampeanas, shows no Tocopilla-related decrease in velocity and is only slightly affected by the 2010 Maule (Weiss et al., 2019) and 2015 earthquakes. The interseismic (i.e., pre-Tocopilla) eastward velocity at TUCU is ~4.7 mm/yr.

Due to the complications in the UNSA time series, we suggest that the site be either excluded from regional analyses, that the earthquake-related time series and velocity perturbations be investigated independently, or that the pre-Tocopilla constant-velocity time interval be used to estimate the interseismic velocity and for comparisons with shortening rates made over longer timescales. Here we take this last approach and generate a new NWA interseismic surface-velocity field and structure-perpendicular velocity profile (Figures 1 and 9) that also includes velocities for four additional CGPS stations (JBAL, TUC1, TERO, and CATA) that are close to our study area and were not analyzed by McFarland et al. (2017) (Figure 1). Our new analysis confirms that horizontal surface velocities decrease gradually toward the foreland and most importantly that there is no definitive rapid decrease in velocity approaching the foreland indicative of a locked décollement beneath the NWA thick-skinned system.

## 5. Discussion

### 5.1. Late Pleistocene Deformation in the Central Calchaquí Valley

Our analysis of structural and stratigraphic data in the central Calchaquí Valley reveals that multiple Late Pleistocene deformation episodes are related to the generation of mesoscale structures in the basin. At least three distinct episodes are recorded in the piedmont of the León Muerto range based on angular unconformities in the Quaternary sediments. The first episode was responsible for the deformation of Units 1–3 as shown in the central and northern profiles; the second episode resulted in the deformation of Unit 4 across the central and southern profiles; and a third episode was responsible for the deformation of Unit 7 across the central and southern profiles (Figure 7). Our kinematic reconstructions suggest that the Quaternary faults in the piedmont of the León Muerto range are high-angle and primarily west verging structures, with the exception of the fault responsible for the deformation of Unit 7 and the fault in the northern profile (Figure S3). We suggest that the Los Castillos fault was reactivated during the Late Pleistocene with slip accommodated by an imbricate fan of "break-back" footwall-shortcut faults (Buchanan & McClay, 1991) (Figure 4b) and that the footwall of the Los Castillos fault would have been weakened due to earlier extension-related deformation associated with overlapping normal faults (Peacock, 2002), thus making this area more susceptible to localized Quaternary shortening.

Footwall shortcuts associated with inverted extensional faults are common features observed in analog deformation models and field settings (Buchanan & McClay, 1991; McClay & Buchanan, 1992). For example, shortcut thrusts have been documented in the footwall of inverted extensional faults in the EC of Argentina (e.g., Carrera & Muñoz, 2008) and they have been described in a similar, inverted structural setting in the EC of Colombia (Mora et al., 2006). The León Muerto shortcut thrusts may be reactivated minor structures of a wide damage zone of a fault or within a transfer zone comprising the El Zorrito-Los Castillos fault system (e.g., Childs et al., 1995; Kley et al., 2005; Peacock, 2002). We suggest that the Quaternary footwall faults affecting strata in the Calchaquí Valley are directly related to inherited and reactivated basement heterogeneities.

Relating the recent, shallow deformation history of the El Mollar area to basement structures is more difficult than to the north. However, the northwest verging Quaternary structures appear to be associated with the NE-SW trending Tertiary syncline in the piedmont of the Cerro Amarillo (Figure 4).

### 5.2. Shortening Rates

Using the Busk fold reconstruction method, we obtained shortening rates ranging from 0.42–2.80 and 0.19–0.26 mm/yr for the León Muerto range piedmont and El Mollar area, respectively (Table 1). We attribute the larger shortening rates in the León Muerto range piedmont as compared to the El Mollar area to

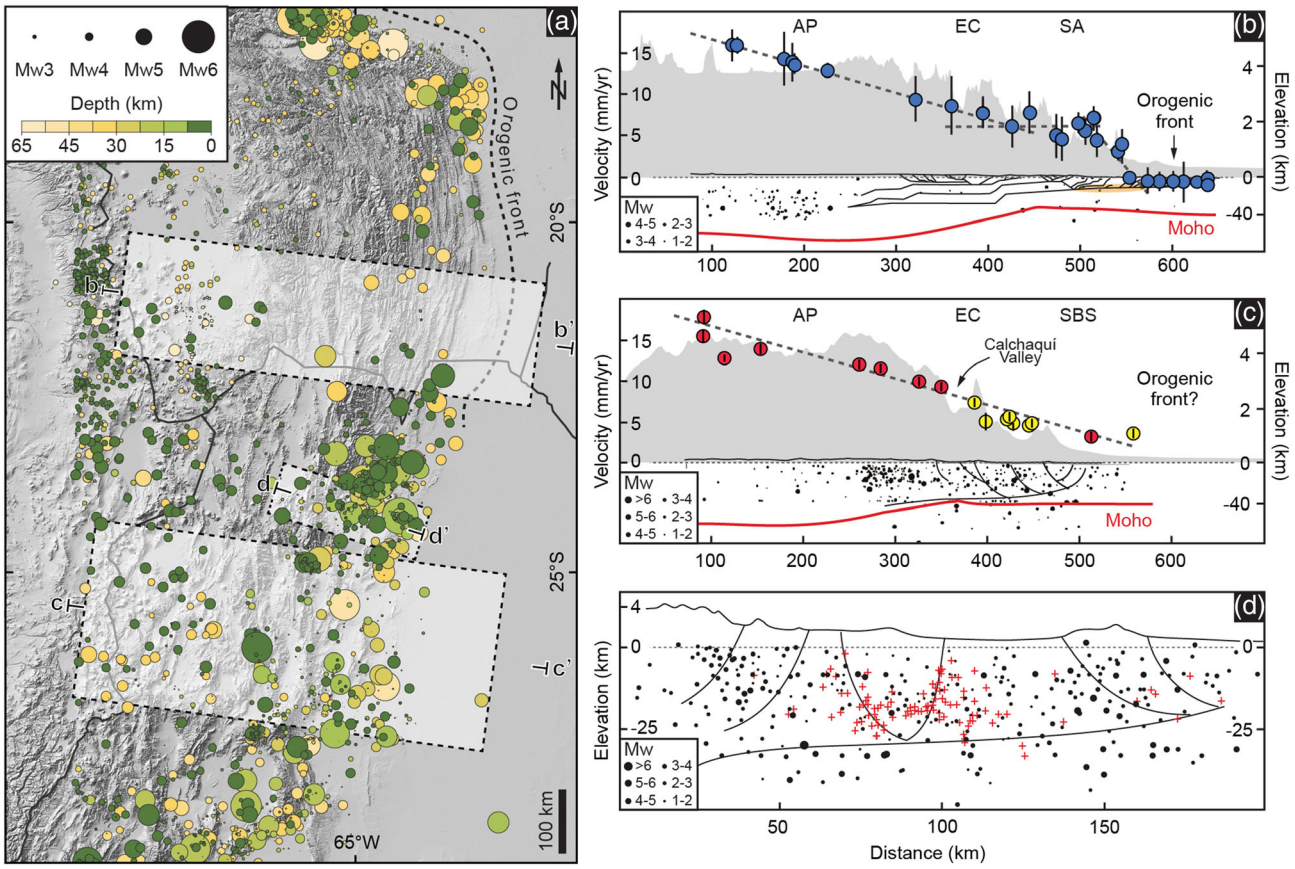


**Figure 10.** Comparison of earthquakes, GPS velocities, and subsurface structures for the eastern margin of the Andean Plateau in southern Bolivia and NWA. (a) Regional seismicity from the International Seismological Center (ISC) for 1987 to 2017. (b and c) The two southern GPS profiles from Figure 1 with projected seismicity from the swaths shown in (a), Moho depth (Laske et al., 2013; Mooney et al., 1998), and subsurface structures modified after Cristallini et al. (2004), Iaffa et al. (2013), Anderson et al. (2017), Ibarra et al. (2019), Liu (2019), and Zeckra (2020). The orange-shaded region in (b) indicates the shallow, inferred locked portion of the décollement (Weiss et al., 2016). (d) Seismicity along the Santa Bárbara System and the Eastern Cordillera. Red crosses indicate the location of events recorded from 1988 to 1989 by the PANDA seismic network (Cahill et al., 1992) and black dots are from the ISC.

the favorable orientation of the structures (N-S in León Muerto range piedmont and NE-SW in El Mollar area) relative to the overall NE-SW regional shortening direction (Cahill et al., 1992) (Figures 1 and 2 and Table 1). In general, our estimates are comparable to the regional shortening rates obtained by García et al. (2013), García et al. (2019), and Ramos et al. (2006), which were calculated without a constrained time period using the time after deposition of the deformed unit, whereas, at least in the León Muerto piedmont, we are able to identify the time interval during which the structures were active.

### 5.3. GPS-Derived Surface Velocities and Distributed Deformation: Thick-Skinned Foreland Versus Thin-Skinned Fold-and-Thrust Belt

In the thin-skinned Subandean fold-and-thrust belt of southern Bolivia, millennial shortening rates appear to be of the same order of magnitude as those determined geodetically (Brooks et al., 2011; Echavarria et al., 2003; Mugnier et al., 2006; Weiss et al., 2016), and Quaternary deformation has mostly been accommodated across a 20- to 40-km-wide wedge-front fault zone (Weiss et al., 2015). Small deviations between rates obtained across different timescales can be attributed to the notion that GPS velocities reflect "instantaneous" deformation of the orogen, which includes both inelastic (i.e., permanent) and elastic deformation, while the geological shortening rates record only permanent deformation (Liu et al., 2000; Shi et al., 2020).

GPS-derived interseismic horizontal surface velocities for the Subandean ranges exhibit a rapid decrease over a short distance (Figure 3). This steep velocity gradient has been interpreted to represent the signal associated with locking on the basal detachment fault (Brooks et al., 2011; Weiss et al., 2016) (Figure 10) and the

accumulation of elastic strain, which will eventually be released during a slip event (i.e., earthquake) and rupture of structures located between the bottom of the locked zone and the wedge-front fault system (Brooks et al., 2011; Weiss et al., 2015, 2016). Approaching the Argentinean border in southern Bolivia, the surface velocities are lower and the rapid gradient is not as steep as toward the north (Figure 3b). Weiss et al. (2016) suggest that this north to south difference might be connected to the recent activity of faults other than those at the wedge front, although it is unclear how these structures behave (i.e., seismic rupture or continuous, aseismic deformation) and might also be related to complications introduced by the presence of multiple active décollements.

Our new GPS results for the thick-skinned deformation belt of NWA, where Quaternary activity is ubiquitous and broadly distributed in time and space (e.g., Casa et al., 2014; García et al., 2013, 2019; Strecker et al., 2012), reveal a gradual decrease in horizontal surface velocities from west to east toward the foreland without the superposed, well-defined, rapid velocity gradient that characterizes the thin-skinned system to the north (Figures 1, 3, and 10). We suggest that this is a reflection of distributed, internal deformation associated with reactivated faults that penetrate the entire brittle crust, comparable to what has been proposed for the fold-and-thrust belts of southern Perú, northern Bolivia, and the thick-skinned Sierras Pampeanas, based on similar GPS surface-velocity patterns (Brooks et al., 2003; Costa et al., 2019; Horton, 1999).

Another noteworthy observation stemming from our geodetic data analysis is that the ≥100-km-wide velocity plateau observed in Bolivia across the EC and west of the aforementioned rapid gradients (Figure 1), interpreted to represent the loading rate at the back of the thin-skinned wedge associated with the freely slipping, downdip portion of the locked, shallow décollement (Weiss et al., 2016), does not characterize the NWA velocity profile. This is important, because the gradual decrease in velocity from the trench to the foreland and the lack of both a velocity plateau and a rapid velocity gradient across our study area point toward different kinematics and imply the lack of an active, shallow décollement.

For the thick-skinned sector of the mountain belt in NWA, the nature, behavior, position, and even presence of a basal décollement is a matter of ongoing debate. Cahill et al. (1992) and Kley and Monaldi (2002) used structural and seismological data to infer the presence of a décollement at a depth of 20–25 km at 24°S (Figure 10). More recently, Ibarra et al. (2019) used a geodynamical model based on geological and geophysical information to show that strain in the EC is concentrated between depths of 30 and 40 km at the transition from the middle to lower crust (Figure 10). South of our study area, in the Sierras Pampeanas, seismological results suggest the presence of a detachment level for the high-angle, basement-involved structures at a depth of ~25 km overlying a more ductile deformation zone (Alvarado & Ramos, 2011; Alvarado et al., 2005; Perarnau et al., 2012; Richardson et al., 2012). This differs from the situation in the thin-skinned system, where both balanced cross sections and inversion of the GPS data indicate the presence of a much shallower, gently dipping décollement in the Paleozoic sediments at 5- to 10-km depth that is thought to control both long- and short-term deformation (Figure 10) (Anderson et al., 2017; Brooks et al., 2011; Dunn et al., 1995; Echavarria et al., 2003; Uba et al., 2009; Weiss et al., 2016).

Geodynamical numerical models focused on the central Andean backarc show that a main factor controlling the difference in structural styles is the pronounced disparity in upper-lithospheric strength between the Bolivian sector of the Andean Plateau (Altiplano) and the foreland when compared to the Puna Plateau and the adjacent broken foreland of the SBS in NWA (e.g., Liu, 2019; Sobolev & Babeyko, 2005). This difference in strength is controlled by the thick sedimentary cover in the Bolivian foreland (Paleozoic to Cenozoic rocks), which thins southward into Argentina (Allmendinger et al., 1983; Horton, 2018; Pearson et al., 2013). As a consequence, simple-shear deformation and the development of a thin-skinned fold and thrust belt above shallow décollement levels within the sedimentary section characterizes southern Bolivia, whereas pure-shear deformation and the absence of suitable detachment levels create a thick-skinned orogenic wedge above a deep-seated décollement in NWA, as had been proposed by Grier et al. (1991).

We suggest that the gentle decrease in horizontal surface velocities across NWA reflects the presence of a 20- to 30-km-deep detachment level in the SBS that deepens to 30–40 km in the EC (Figure 10). Interestingly, this depth range also corresponds with the lower limit of concentrated deep crustal earthquakes (Zeckra, 2020) (Figure 10). It is thus feasible that the thick-skinned structures detach at these depths, resulting in sustained, spatiotemporally unsystematic tectonic activity across the NWA backarc. In such a scenario, the widespread distribution of Quaternary structures and associated tectonic landforms would be

the near-surface manifestation of this style of deformation (Arnous et al., 2020; Ramos et al., 2006). In this context, the north to south changes in the decadal-scale surface-velocity patterns in southern Bolivia and NWA reflect the transition from a well-defined, locked décollement that controls a more systematic, generally in-sequence evolution of surface deformation (e.g., Uba et al., 2009) to a thick-skinned system with no locked décollement and where deformation is broadly distributed across the orogen (e.g., Hilley et al., 2005). In the latter structural setting (i.e., the SBS), contemporaneous crustal deformation and strain release occur across active structures in a highly disorganized manner and at different spatial scales, some of which may occur at different crust levels (Abascal, 2005).

The surface expression of this deformation is related to widely distributed but localized (i.e., short in map view compared to the Subandes) structures, and therefore, the shortening rates observed across the thick-skinned system will be highly variable and might never equate to the GPS-derived shortening. Thus, a direct comparison of the millennial shortening rates associated with individual structures and the overall surface velocities in NWA is not as straightforward as in the Subandean fold-and-thrust belt. Only after obtaining detailed information on the shortening rates associated with all of the active structures for comparable time intervals would it be possible to calculate cumulative geologic shortening rates that are comparable to the geodetic estimates. For example, Pearson et al. (2013) presented a comprehensive cross section through the thick-skinned fold-and-thrust belt of NWA and obtained shortening rates of 1.9 mm/yr from 40 to 12 Myr and 6.5 mm/yr from 12 to 4 Myr in the EC and 5.3 mm/yr in the SBS from 4 to 0 Myr. These rates are similar to those obtained from the GPS data but at least twice as large as our measurements across structures in the central Calchaquí Valley. The structures and deformation features in the alluvial-fan surfaces of the central Calchaquí Valley thus correspond to a limited sector of tectonic activity in the overall deformation space in the transition between the EC and the SBS. Importantly, neighboring mountain fronts are inactive on timescales similar to those in our analysis, while other areas in this region may be tectonically active, but a more voracious erosional regime (e.g., Arnous et al., 2020) does not allow for the preservation of tectonic landforms and structures.

The differences in the accommodation of deformation between the thin- and thick-skinned fold-and-thrust belts of the southern Central Andes also impact regional seismicity and hazard. In the Bolivian Subandean ranges, recent work suggests the possibility of infrequent great earthquakes ($>M_w$ 8.0) that may rupture the entire locked portion of the décollement, similar to what occurs along the Himalayan mountain front (Bilham, 2019; Kumar et al., 2010; Wesnousky, 2020). This assessment for the Bolivian Subandes has been made in the absence of both paleoseismological investigations and historical records of large, ground-rupturing earthquakes. Rather, the suggestion of infrequent large earthquakes rupturing the Subandean mountain front is based on inferences related to the rapid surface-velocity gradient, the perplexing lack of recent seismicity (i.e., accumulating strain is not being released by lower magnitude earthquakes; Figure 10), and the along-strike continuity and morphology of tectonic structures that include the frontal-thrust fault system (Brooks et al., 2011; Shi et al., 2020; Weiss et al., 2016). In contrast, widely distributed and frequent small- to intermediate-magnitude ($M_w$ 2.0–7.0), and sometimes destructive, earthquakes characterize NWA (Figures 1 and 9). This widespread crustal seismicity, in combination with the shorter along-strike extent of tectonic structures (Figures 1 and 2), the numerous, relatively slowly deforming Quaternary structures throughout the region, and the lack of a definitive, well-defined geodetic velocity gradient, suggests that great earthquakes are less likely to occur on the inverted structures in the thick-skinned SBS and are perhaps mechanically implausible (i.e., no shallow décollement).

## 6. Conclusions

New Quaternary shortening rates for thrust fault-related structures in the central Calchaquí Valley, NWA, combined with revised GPS-derived surface velocities and compared to the distribution of crustal seismicity (Figure 10), support the notion that deformation across the thick-skinned southern Central Andes is widely distributed. This style of deformation has characterized the region for millions of years, making direct comparisons of field-based Quaternary shortening rates and those determined geodetically difficult. Ongoing deformation is primarily concentrated in the intermontane valleys and, judging by the currently available temporal resolution of Quaternary regional deformation episodes, it can be inferred that many structures have been simultaneously active on millennial to centennial timescales, which is compatible with the

widely distributed present-day and historical NWA seismicity. In the central Calchaquí Valley, Quaternary deformation is accommodated by high-angle faults and associated folds that were active during at least three separate deformation episodes and are associated with the valley border faults. According to our reconstruction of the deformation history of these shallow structures, the driver for this style of neotectonic activity is the compressional reactivation of deep-seated, extensional faults inherited from Cretaceous rifting. The style of deformation in the SBS and EC of NWA is characterized by a combination of widely distributed, thick- and thin-skinned deformation processes that are compatible with the gradual eastward decrease in GPS-derived horizontal surface velocities and the present-day seismicity. This behavior is fundamentally different from that of the thin-skinned Subandean fold-and-thrust belt of southern Bolivia and northern Argentina where geodesy, limited crustal seismicity, and the distribution of Quaternary deformation structures point toward elevated seismic hazard and the possibility of large earthquakes with unknown recurrence intervals.

## Data Availability Statement

New OSL age data and GPS velocities presented in the figures and tables of the main text and supporting information and can be found online (at https://osf.io/2vztw). Additional GPS velocities and associated data used to create Figures 1 and 10 can be found in Weiss et al. (2016) and McFarland et al. (2017). OSL ages for the El Mollar Area come from Reger (2018).

**Acknowledgments**

We are grateful to Jonas Kley and Carlos Costa for providing thorough and thoughtful comments that helped improve the clarity of the manuscript. We thank Carolin Reger and Alexander Fülling for assistance with OSL sample preparation and dating. We also thank Henry Wichura, Verónica Torres, and A. Gutierrez for their logistical and administrative support. We are grateful to Corinna Kallich for helping draft the figures. We thank James Foster, Eric Kendrick, and Mike Bevis for their ongoing support with South America GPS data processing and analysis. We also thank Rick Bennett and Philip McFarland for installing and maintaining the PAGA CGPS network in NWA and UNAVCO for serving the associated data. This research was funded by CONICET (Consejo Nacional de Investigaciones Científicas y Técnicas), through the projects PUE-IBIGEO 22920160100108CO, PICT 1928, and CIUNSa 2336. This work was co-funded by the German Research Foundation (DFG) grant 373/34-1 to M. S. and the Brandenburg Ministry of Sciences, Research and Cultural Affairs, Germany, within the framework of the International Research Training Group IGK2018 SuRfAce processes, Tectonics and Georesources: The Andean foreland basin of Argentina (StRATEGy). We thank the German-Argentine University Network (DAHZ/CUAA; grant to M. S. and A. Gutierrez: Riesgos Naturales), the Deutscher Akademischer Austauschdienst and CONICET for their funding and support of S. F. J. R. W was partially supported by the Natural Environmental Research Council (NERC) through the Centre for the Observation and Modeling of Earthquakes, Volcanoes and Tectonics.

## References

Abascal, L. D. V. (2005). Combined thin-skinned and thick-skinned deformation in the central Andean foreland of northwestern Argentina. *Journal of South American Earth Sciences*, *19*(1), 75–81. https://doi.org/10.1016/j.jsames.2005.01.004

Allmendinger, R. W., Ramos, V. A., Jordan, T. E., Palma, M., & Isacks, B. L. (1983). Paleogeography and Andean structural geometry, northwest Argentina. *Tectonics*, *2*(1), 1–16. https://doi.org/10.1029/TC002i001p00001

Alvarado, P., Machuca, B., & Beck, S. (2005). Comparative seismic and petrographic crustal study between the Western and Eastern Sierras Pampeanas region (31°S). *Revista de la Asociacion Geologica Argentina*, *60*, 787–796.

Alvarado, P., & Ramos, V. (2011). Earthquake deformation in the northwestern Sierras Pampeanas of Argentina based on seismic waveform modeling. *Journal of Geodynamics*, *51*(4), 205–218. https://doi.org/10.1016/j.jog.2010.08.002

Anderson, R. B., Long, S. P., Horton, B. K., Calle, A. Z., & Ramirez, V. (2017). Shortening and structural architecture of the Andean fold-thrust belt of southern Bolivia (21°S): Implications for kinematic development and crustal thickening of the central Andes. *Geosphere*, *13*(2), 538–558. https://doi.org/10.1130/GES01433.1

Arnous, A., Zeckra, M., Venerdini, A., Alvarado, P., Arrowsmith, R., Guillemoteau, J., et al. (2020). Neotectonic activity in the low-strain broken foreland (Santa Bárbara System) of the North-Western Argentinean Andes (26°S). *Lithosphere*, *2020*(1), 1–25. https://doi.org/10.2113/2020/8888588

Avouac, J. P. (2008). Dynamic processes in extensional and compressional Settings-Mountain building: From earthquakes to geological deformation. *Treatise on Geophysics*, *6*, 377–439.

Bilham, R. (2019). Himalayan earthquakes: A review of historical seismicity and early 21st century slip potential. *Geological Society, London, Special Publications*, *483*(1), 423–482. https://doi.org/10.1144/SP483.16

Brooks, B. A., Bevis, M., Smalley, R. J., Kendrick, E., Manceda, R., Lauria, E., et al. (2003). Crustal motion in the southern Andes (26°–36°S): Do the Andes behave like a microplate? *Geochemistry, Geophysics, Geosystems*, *4*(10), 1085. https://doi.org/10.1029/2003GC000505

Brooks, B. A., Bevis, M., Whipple, K., Ramon Arrowsmith, J., Foster, J., Zapata, T., et al. (2011). Orogenic-wedge deformation and potential for great earthquakes in the central Andean backarc. *Nature Geoscience*, *4*(6), 380–383. https://doi.org/10.1038/ngeo1143

Buchanan, P. G., & McClay, K. R. (1991). Sandbox experiments of inverted listric and planar fault systems. *Tectonophysics*, *188*(1–2), 97–115. https://doi.org/10.1016/0040-1951(91)90317-L

Busk, H. G. (1929). *Earth flexures*. Cambridge: Cambridge University Press.

Büttner, S. H., Glodny, J., Lucassen, F., Wemmer, K., Erdmann, S., Handler, R., & Franz, G. (2005). Ordovician metamorphism and plutonism in the Sierra de Quilmes metamorphic complex: Implications for the tectonic setting of the northern Sierras Pampeanas (NW Argentina). *Lithos*, *83*(1–2), 143–181. https://doi.org/10.1016/j.lithos.2005.01.006

Cahill, T., Isacks, B. L., Whitman, D., Chatelain, J.-L., Perez, A., & Chiu, J. M. (1992). Seismicity and tectonics in Jujuy Province, northwestern Argentina. *Tectonics*, *11*(5), 944–959. https://doi.org/10.1029/92TC00215

Carrera, N., & Muñoz, J. A. (2008). Thrusting evolution in the southern Cordillera Oriental (northern Argentine Andes): Constraints from growth strata. *Tectonophysics*, *459*(1–4), 107–122. https://doi.org/10.1016/j.tecto.2007.11.068

Carrera, N., & Muñoz, J. A. (2013). Thick-skinned tectonic style resulting from the inversion of previous structures in the southern Cordillera Oriental (NW Argentine Andes). *Geological Society, London, Special Publications*, *377*(1), 77–100. https://doi.org/10.1144/SP377.2

Carrera, N., Muñoz, J. A., Sàbat, F., Mon, R., & Roca, E. (2006). The role of inversion tectonics in the structure of the Cordillera Oriental (NW Argentinean Andes). *Journal of Structural Geology*, *28*(11), 1921–1932. https://doi.org/10.1016/j.jsg.2006.07.006

Casa, A., Yamin, M., Cegarra, M., Wright, E., Coppolecchia, M., Costa, C., et al. (2014). Actualización del SIG de las Deformaciones Cuaternarias de la República Argentina, in *XIX Congreso Geológico Argentino*, edited, Córdoba, Argentina.

Childs, C., Watterson, J., & Walsh, J. J. (1995). Fault overlap zones within developing normal fault systems. *Journal of the Geological Society*, *152*(3), 535–549. https://doi.org/10.1144/gsjgs.152.3.0535

Costa, C. H., Owen, L. A., Ricci, W. R., Johnson, W. J., & Halperin, A. D. (2018). Holocene activity and seismogenic capability of intraplate thrusts: Insights from the Pampean Ranges. *Argentina, Tectonophysics*, *737*, 57–70. https://doi.org/10.1016/j.tecto.2018.05.002

Costa, C. H., Schoenbohm, L. M., Brooks, B. A., Gardini, C. E., & Richard, A. D. (2019). Assessing Quaternary shortening rates at an Andean Frontal Thrust (32°30′S), Argentina. *Tectonics*, *38*, 3034–3051. https://doi.org/10.1029/2019TC005564

Cristallini, E., Cominguez, A., Ramos, V., & Mercerat, E. (2004). Basement double-wedge thrusting in the Northern Sierras Pampeanas of Argentina (27°S)—Constraints from deep seismic reflection, edited, pp. 65–90.

Dahlstrom, C. D. A. (1969). Balanced cross sections. *Canadian Journal of Earth Sciences*, *6*(4), 743–757. https://doi.org/10.1139/e69-069

DeCelles, P. G., & Giles, K. A. (1996). Foreland basin systems. *Basin Research*, *8*(2), 105–123. https://doi.org/10.1046/j.1365-2117.1996.01491.x

del Papa, C., Hongn, F., Powell, J., Payrola, P., Do Campo, M., Strecker, M. R., et al. (2013). Middle Eocene-Oligocene broken-foreland evolution in the Andean Calchaqui Valley, NW Argentina: Insights from stratigraphic, structural and provenance studies. *Basin Research*, *25*(5), 574–593. https://doi.org/10.1111/bre.12018

Delouis, B., Pardo, M., Legrand, D., & Monfret, T. (2009). The *Mw* 7.7 Tocopilla earthquake of 14 November 2007 at the southern edge of the northern Chile seismic gap: Rupture in the deep part of the coupled plate interface. *Bulletin of the Seismological Society of America*, *99*(1), 87–94.

Dunn, J. F., Hartshorn, K. G., & Hartshorn, P. W. (1995). Structural styles and hydrocarbon potential of the sub-Andean thrust belt of southern Bolivia. In A. J. Tankard, R. S. Soruco, H. J. Welsink (Eds.), *Petroleum Basins of South America* (pp. 523–543). Santa Cruz, Bolivia: The American Association of Petroleum Geologists.

Echavarria, L., Hernandez, R., Allmendinger, R., & Reynolds, J. (2003). Subandean thrust and fold belt of northwestern Argentina: Geometry and timing of the Andean evolution. *AAPG Bulletin*, *87*(6), 965–985. https://doi.org/10.1306/01200300196

Eude, A., Roddaz, M., Brichau, S., Brusset, S., Calderon, Y., Baby, P., & Soula, J.-C. (2015). Controls on timing of exhumation and deformation in the northern Peruvian eastern Andean wedge as inferred from low-temperature thermochronology and balanced cross section. *Tectonics*, *34*, 715–730. https://doi.org/10.1002/2014TC003641

Gallardo, E. F. (1988). Geología del Cuaternario en la confluencia de los ríos Calchaquí y Santa María (Salta). *Revista de la Asociación Geológica Argentina*, *4*, 435–444.

García, V. H., Hongn, F., & Cristallini, E. O. (2013). Late Miocene to recent morphotectonic evolution and potential seismic hazard of the northern Lerma valley: Clues from Lomas de Medeiros. *Cordillera Oriental, NW Argentina, Tectonophysics*, *608*, 1238–1253.

García, V. H., Hongn, F., Yagupsky, D., Pingel, H., Kinnaird, T., Winocur, D., et al. (2019). Late Quaternary tectonics controlled by fault reactivation. Insights from a local transpressional system in the intermontane Lerma valley, Cordillera Oriental, NW Argentina. *Journal of Structural Geology*, *128*, 103875.

González Bonorino, F. (1950a). Geologic cross-section of the Cordillera de los Andes at about parallel 33° L.S. (Argentina-Chile). *GSA Bulletin*, *61*(1), 17–26. https://doi.org/10.1130/0016-7606(1950)61[17:GCOTCD]2.0.CO;2

González Bonorino, F. (1950b). Algunos problemas geológicos de las Sierras Pampeanas. *Revista de la Asociación Geológica Argentina*, *5*(3), 81–110.

Grandin, R., Klein, E., Métois, M., & Vigny, C. (2016). Three-dimensional displacement field of the 2015 *Mw*8.3 Illapel earthquake (Chile) from across- and along-track Sentinel-1 TOPS interferometry. *Geophysical Research Letters*, *43*, 2552–2561. https://doi.org/10.1002/2016GL067954

Grier, M. E., Salfity, J. A., & Allmendinger, R. W. (1991). Andean reactivation of the Cretaceous Salta rift, northwestern Argentina. *Journal of South American Earth Sciences*, *4*(4), 351–372. https://doi.org/10.1016/0895-9811(91)90007-8

Hain, M. P., Strecker, M. R., Bookhagen, B., Alonso, R. N., Pingel, H., & Schmitt, A. K. (2011). Neogene to Quaternary broken foreland formation and sedimentation dynamics in the Andes of NW Argentina (25°S). *Tectonics*, *30*, TC2006. https://doi.org/10.1029/2010TC002703

Hayes, G. P., Moore, G. L., Portner, D. E., Hearne, M., Flamme, H., Furtney, M., & Smoczyk, G. M. (2018). Slab2, a comprehensive subduction zone geometry model. *Science*, *362*(6410), 58–61. https://doi.org/10.1126/science.aat4723

Hermanns, R. L., & Niedermann, S. (2011). Late Pleistocene–early Holocene paleoseismicity deduced from lake sediment deformation and coeval landsliding in the Calchaquíes valleys, NW Argentina. In A. Franck, M. Audemard, M. M. Alessandro, J. P. McCalpin (Eds.), *Geological criteria for evaluating seismicity revisited: Forty years of paleoseismic investigations and the natural record of past earthquakes*. Colorado, United States of America: Geological Society of America.

Hermanns, R. L., Niedermann, S., Ivy-Ochs, S., & Kubik, P. W. (2004). Rock avalanching into a landslide-dammed lake causing multiple dam failure in Las Conchas valley (NW Argentina)—Evidence from surface exposure dating and stratigraphic analyses. *Landslides*, *1*(2), 113–122.

Hermanns, R. L., & Strecker, M. R. (1999). Structural and lithological controls on large Quaternary rock avalanches (sturzstroms) in arid northwestern Argentina. *GSA Bulletin*, *111*(6), 934–948. https://doi.org/10.1130/0016-7606(1999)111<0934:SALCOL>2.3.CO;2

Hilley, G. E., Blisniuk, P. M., & Strecker, M. R. (2005). Mechanics and erosion of basement-cored uplift provinces. *Journal of Geophysical Research*, *110*, B12409. https://doi.org/10.1029/2005JB003704

Hongn, F., Mon, R., Petrinovic, I., del Papa, C., & Powell, J. (2010). Inversión y reactivación tectónicas cretácicocenozoicas en el Noroeste Argentino: Influencia de las heterogeneidades del basamento neoproterozoico-paleozoico inferior. *Revista de la Asociación Geológica Argentina*, *66*, 38–53.

Horton, B. K. (1999). Erosional control on the geometry and kinematics of thrust belt development in the central Andes. *Tectonics*, *18*(6), 1292–1304. https://doi.org/10.1029/1999TC900051

Horton, B. K. (2018). Sedimentary record of Andean mountain building. *Earth-Science Reviews*, *178*, 279–309. https://doi.org/10.1016/j.earscirev.2017.11.025

Hubbard, J., Barbot, S., Hill, E. M., & Tapponnier, P. (2015). Coseismic slip on shallow décollement megathrusts: Implications for seismic and tsunami hazard. *Earth-Science Reviews*, *141*, 45–55. https://doi.org/10.1016/j.earscirev.2014.11.003

Iaffa, D., Sàbat, F., Muñoz, J., & Carrera, N. (2013). Basin fragmentation controlled by tectonic inversion and basement uplift in Sierras Pampeanas and Santa Bárbara System, northwest Argentina. *Geological Society London Special Publications*, *377*(1), 101–117. https://doi.org/10.1144/SP377.13

Iaffa, D. N., Sàbat, F., Muñoz, J. A., Mon, R., & Gutierrez, A. A. (2011). The role of inherited structures in a foreland basin evolution. The Metán Basin in NW Argentina. *Journal of Structural Geology*, *33*(12), 1816–1828. https://doi.org/10.1016/j.jsg.2011.09.005

Ibarra, F., Liu, S., Meeßen, C., Prezzi, C. B., Bott, J., Scheck-Wenderoth, M., et al. (2019). 3D data-derived lithospheric structure of the Central Andes and its implications for deformation: Insights from gravity and geodynamic modelling. *Tectonophysics*, *766*, 453–468. https://doi.org/10.1016/j.tecto.2019.06.025

Jordan, T. E. (1981). Thrust loads and foreland basin evolution, Cretaceous, western United States. *AAPG Bulletin*, *65*(12), 2506–2520.

Jordan, T. E., & Allmendinger, R. W. (1986). The Sierras Pampeanas of Argentina; a modern analogue of Rocky Mountain foreland deformation. *American Journal of Science*, *286*(10), 737–764. https://doi.org/10.2475/ajs.286.10.737

Jordan, T. E., Isacks, B. L., Allmendinger, R. W., Brewer, J. A., Ramos, V. A., & Ando, C. J. (1983). Andean tectonics related to geometry of subducted Nazca plate. *GSA Bulletin*, *94*(3), 341–361. https://doi.org/10.1130/0016-7606(1983)94<341:ATRTGO>2.0.CO;2

Kley, J., & Monaldi, C. R. (2002). Tectonic inversion in the Santa Barbara System of the central Andean foreland thrust belt, northwestern Argentina. *Tectonics*, *21*(6), 1061. https://doi.org/10.1029/2002TC902003

Kley, J., Monaldi, C. R., & Salfity, J. A. (1999). Along-strike segmentation of the Andean foreland: Causes and consequences. *Tectonophysics*, *301*(1–2), 75–94. https://doi.org/10.1016/S0040-1951(98)90223-2

Kley, J., Rossello, E. A., Monaldi, C. R., & Habighorst, B. (2005). Seismic and field evidence for selective inversion of Cretaceous normal faults, Salta rift, northwest Argentina. *Tectonophysics*, *399*(1–4), 155–172. https://doi.org/10.1016/j.tecto.2004.12.020

Kumar, S., Wesnousky, S. G., Jayangondaperumal, R., Nakata, T., Kumahara, Y., & Singh, V. (2010). Paleoseismological evidence of surface faulting along the northeastern Himalayan front, India: Timing, size, and spatial extent of great earthquakes. *Journal of Geophysical Research*, *115*, B12422. https://doi.org/10.1029/2009JB006789

Laske, G., Masters, G., Ma, Z., & Pasyanos, M. (2013). Update on CRUST1.0—A 1-degree global model of Earth's crust, Abstract EGU2013–2658 presented at 2013. *Geophysical Research Abstracts*, *15*(15), 2658.

Liu, M., Yang, Y., Stein, S., Zhu, Y., & Engeln, J. (2000). Crustal shortening in the Andes: Why do GPS rates differ from geological rates? *Geophysical Research Letters*, *27*(18), 3005–3008. https://doi.org/10.1029/2000GL008532

Liu, S. (2019). *Controls of foreland-deformation patterns in the orogen-foreland shortening system* (p. 161). Potsdam, Germany: University of Potsdam.

Marquillas, R. A., del Papa, C., & Sabino, I. F. (2005). Sedimentary aspects and paleoenvironmental evolution of a rift basin: Salta Group (Cretaceous–Paleogene), northwestern Argentina. *International Journal of Earth Sciences*, *94*(1), 94–113. https://doi.org/10.1007/s00531-004-0443-2

Marshak, S., Karlstrom, K., & Timmons, J. M. (2000). Inversion of Proterozoic extensional faults: An explanation for the pattern of Laramide and Ancestral Rockies intracratonic deformation, United States. *Geology*, *28*(8), 735–738. https://doi.org/10.1130/0091-7613(2000)28<735:IOPEFA>2.0.CO;2

McClay, K. R., & Buchanan, P. G. (1992). Thrust faults in inverted extensional basins. In K. R. McClay (Ed.), *Thrust tectonics* (pp. 93–104). Dordrecht: Springer Netherlands. https://doi.org/10.1007/978-94-011-3066-0_8

McFarland, P. K., Bennett, R. A., Alvarado, P., & DeCelles, P. G. (2017). Rapid geodetic shortening across the Eastern Cordillera of NW Argentina observed by the Puna-Andes GPS Array. *Journal of Geophysical Research: Solid Earth*, *122*, 8600–8623. https://doi.org/10.1002/2017JB014739

McQuarrie, N., Barnes, J. B., & Ehlers, T. A. (2008). Geometric, kinematic, and erosional history of the central Andean Plateau, Bolivia (15–17°S). *Tectonics*, *27*, TC3007. https://doi.org/10.1029/2006TC002054

Mon, R., & Salfity, J. A. (1995). Tectonic evolution of the Andes of northern Argentina. In A. J. Tankard, R. S. Soruco, H. J. Welsink (Eds.), *Petroleum basins of South America* (pp. 269–283). Tulsa, United States of America: American Association of Petroleum Geologists.

Mooney, W. D., Laske, G., & Masters, T. G. (1998). CRUST 5.1: A global crustal model at 5 × 5. *Journal of Geophysical Research*, *103*(B1), 727–747.

Mora, A., Parra, M., Strecker, M. R., Kammer, A., Dimaté, C., & Rodríguez, F. (2006). Cenozoic contractional reactivation of Mesozoic extensional structures in the Eastern Cordillera of Colombia. *Tectonics*, *25*, TC2010. https://doi.org/10.1029/2005TC001854

Mortimer, E., Carrapa, B., Coutand, I., Schoenbohm, L., Sobel, E. R., Sosa Gomez, J., & Strecker, M. R. (2007). Fragmentation of a foreland basin in response to out-of-sequence basement uplifts and structural reactivation: El Cajón-Campo del Arenal basin, NW Argentina. *GSA Bulletin*, *119*(5–6), 637–653. https://doi.org/10.1130/B25884.1

Mugnier, J.-L., Becel, D., & Granjeon, D. (2006). Active tectonics in the Subandean belt inferred from the morphology of the Rio Pilcomayo (Bolivia). *GSA Special Paper*, *398*, 353–369.

Norabuena, E., Leffler-Griffin, L., Mao, A., Dixon, T., Stein, S., Sacks, I. S., et al. (1998). Space geodetic observations of Nazca-South America convergence across the Central Andes. *Science*, *279*(5349), 358–362. https://doi.org/10.1126/science.279.5349.358

Peacock, D. C. P. (2002). Propagation, interaction and linkage in normal fault systems. *Earth Science Reviews*, *58*(1–2), 121–142. https://doi.org/10.1016/S0012-8252(01)00085-X

Pearson, D. M., Kapp, P., DeCelles, P. G., Reiners, P. W., Gehrels, G. E., Ducea, M. N., & Pullen, A. (2013). Influence of pre-Andean crustal structure on Cenozoic thrust belt kinematics and shortening magnitude: Northwestern Argentina. *Geosphere*, *9*(6), 1766–1782. https://doi.org/10.1130/GES00923.1

Perarnau, M., Gilbert, H., Alvarado, P., Martino, R., & Anderson, M. (2012). Crustal structure of the Eastern Sierras Pampeanas of Argentina using high frequency local receiver functions. *Tectonophysics*, *580*, 208–217. https://doi.org/10.1016/j.tecto.2012.09.021

Ramos, V. A. (2017). Las provincias geológicas del noroeste argentino. In C. M. Muruaga & P. Grosse (Eds.), *Ciencias de la Tierra y Recursos Naturales del NOA, Relatorio del XX Congreso Geológico Argentino* (pp. 38–52). San Miguel de Tucumán, Argentina: Relatorio del XX Congreso Geológico Argentino.

Ramos, V. A., Alonso, R., & Strecker, M. (2006). Estructura y neotectónica de Las Lomas de Olmedo, zona de transición entre los Sistemas Subandino y de Santa Bárbara, provincia de Salta. *Revista de la Asociacion Geologica Argentina*, *61*, 579–588.

Reger, C. (2018). *Dating of alluvial fans from NW Argentina using cosmogenic nuclides and optically stimulated luminescence technique*. Potsdam, Germany: University of Potsdam.

Reynolds, J. H., Galli, C. I., Hernández, R. M., Idleman, B. D., Kotila, J. M., Hilliard, R. V., & Naeser, C. W. (2000). Middle Miocene tectonic development of the Transition Zone, Salta Province, northwest Argentina: Magnetic stratigraphy from the Metán Subgroup, Sierra de González. *GSA Bulletin*, *112*(11), 1736–1751. https://doi.org/10.1130/0016-7606(2000)112<1736:MMTDOT>2.0.CO;2

Richardson, T., Gilbert, H., Anderson, M., & Ridgway, K. D. (2012). Seismicity within the actively deforming Eastern Sierras Pampeanas, Argentina. *Geophysical Journal International*, *188*(2), 408–420. https://doi.org/10.1111/j.1365-246X.2011.05283.x

Scott, C., Lohman, R., Pritchard, M., Alvarado, P., & Sánchez, G. (2014). Andean earthquakes triggered by the 2010 Maule, Chile (mw 8.8) earthquake: Comparisons of geodetic, seismic and geologic constraints. *Journal of South American Earth Sciences*, *50*, 27–39. https://doi.org/10.1016/j.jsames.2013.12.001

Shi, F., Li, S., & Moreno, M. (2020). Megathrust locking and viscous mantle flow induce continental shortening in Central Andes. *Pure and Applied Geophysics*, *177*(6), 2841–2852, https://doi.org/10.1007/s00024-019-02403-0

Sobolev, S. V., & Babeyko, A. Y. (2005). What drives orogeny in the Andes? *Geology*, *33*(8), 617–620. https://doi.org/10.1130/G21557AR.1

Storchak, D. A., Di Giacomo, D., Bondár, I., Engdahl, E. R., Harris, J., Lee, W. H. K., et al. (2013). Public release of the ISC-GEM global instrumental earthquake catalogue (1900–2009). *Seismological Research Letters*, *84*(5), 810–815. https://doi.org/10.1785/0220130034

Strecker, M. R., Alonso, R. N., Bookhagen, B., Carrapa, B., Hilley, G. E., Sobel, E. R., & Trauth, M. H. (2007). Tectonics and climate of the southern Central Andes. *Annual Review of Earth and Planetary Sciences*, *35*(1), 747–787. https://doi.org/10.1146/annurev.earth.35.031306.140158

Strecker, M. R., Hilley, G. E., Bookhagen, B., & Sobel, E. R. (2012). Structural, geomorphic, and depositional characteristics of contiguous and broken foreland basins: Examples from the eastern flanks of the Central Andes in Bolivia and NW Argentina, in *Tectonics of Sedimentary Basins*, edited, pp. 508–521.

Strecker, M. R., & Marrett, R. (1999). Kinematic evolution of fault ramps and its role in development of landslides and lakes in the northwestern Argentine Andes. *Geology*, *27*(4), 307–310. https://doi.org/10.1130/0091-7613(1999)027<0307:KEOFRA>2.3.CO;2

Torres, M. (1985). Estratigrafía de la ladera occidental del cerro Amarillo y Quebrada de La Yesera. Departamento de Cafayate, Salta. *Revista de la Asociación Geológica Argentina*, *40*(3–4), 141–157.

Uba, C. E., Kley, J., Strecker, M., & Schmitt, A. K. (2009). Unsteady evolution of the Bolivian Subandean thrust belt: The role of enhanced erosion and clastic wedge progradation. *Earth and Planetary Science Letters*, *281*(3–4), 134–146. https://doi.org/10.1016/j.epsl.2009.02.010

Villegas-Lanza, J. C., Chlieh, M., Cavalié, O., Tavera, H., Baby, P., Chire-Chira, J., & Nocquet, J. M. (2016). Active tectonics of Peru: Heterogeneous interseismic coupling along the Nazca megathrust, rigid motion of the Peruvian Sliver, and Subandean shortening accommodation. *Journal of Geophysical Research: Solid Earth*, *121*, 7371–7394. https://doi.org/10.1002/2016JB013080

Weiss, J. R., Brooks, B. A., Arrowsmith, J. R., & Vergani, G. (2015). Spatial and temporal distribution of deformation at the front of the Andean orogenic wedge in southern Bolivia. *Journal of Geophysical Research: Solid Earth*, *120*, 1909–1931. https://doi.org/10.1002/2014JB011763

Weiss, J. R., Brooks, B. A., Foster, J. H., Bevis, M., Echalar, A., Caccamise, D., et al. (2016). Isolating active orogenic wedge deformation in the southern Subandes of Bolivia. *Journal of Geophysical Research: Solid Earth*, *121*, 6192–6218. https://doi.org/10.1002/2016JB013145

Weiss, J. R., Qiu, Q., Barbot, S., Wright, T. J., Foster, J. H., Saunders, A., et al. (2019). Illuminating subduction zone rheological properties in the wake of a giant earthquake. *Science Advances*, *5*(12), eaax6720.

Wesnousky, S. G. (2020). Great pending Himalaya earthquakes. *Seismological Research Letters*, *91*(6), 3334–3342. https://doi.org/10.1785/0220200200

Zeckra, M. (2020). *Seismological and Seismotectonic Analysis of the Northwestern Argentine Central Andean Foreland*. Potsdam, German: University of Potsdam.

## References From the Supporting Information

Buylaert, J.-P., Murray, A., Thomsen, K., & Jain, M. (2009). Testing the potential of an elevated temperature IRSL signal from K-feldspar. *Radiation Measurements - RADIAT MEAS*, *44*(5–6), 560–565. https://doi.org/10.1016/j.radmeas.2009.02.007

Murray, A., & Wintle, A. G. (2000). Dating quartz using an improved single-aliquot regenerative-dose (SAR) protocol. *Radiation Measurements*, *32*(1), 57–73. https://doi.org/10.1016/S1350-4487(99)00253-X

Wallinga, J. (2002). Optically stimulated luminescence dating of fluvial deposits: A review. *Boreas*, *31*(4), 303–322. https://doi.org/10.1080/030094802320942536